


SHORT COMMUNICATION **OPEN ACCESS**

Human Transmembrane Serine Protease 2 (TMPRSS2) on Human Seminal Fluid Extracellular Vesicles Is Proteolytically Active

Emile Verhulst¹  | Michelle De Bruyn¹ | Pascale Berckmans² | Yani Sim¹ | Koen Augustyns^{3,6} | Isabel Pintelon^{4,5} | Maya Berg⁶ | Pieter Van Wielendaele¹ | Anne-Marie Lambeir¹ | Yann G.-J. Sterckx¹ | Inge Nelissen² | Ingrid De Meester^{1,6}

¹Laboratory of Medical Biochemistry, Faculty of Pharmaceutical, Biomedical and Veterinary Sciences, University of Antwerp, Wilrijk, Belgium | ²Health Unit, Flemish Institute for Technological Research, Mol, Belgium | ³Laboratory of Medicinal Chemistry, Faculty of Pharmaceutical, Biomedical and Veterinary Sciences, University of Antwerp, Wilrijk, Belgium | ⁴Laboratory of Cell Biology and Histology, Faculty of Pharmaceutical, Biomedical and Veterinary Sciences, University of Antwerp, Wilrijk, Belgium | ⁵Antwerp Centre for Advanced Microscopy (ACAM), Faculty of Pharmaceutical, Biomedical and Veterinary Sciences, University of Antwerp, Wilrijk, Belgium | ⁶Infla-Med Centre of Excellence, University of Antwerp, Wilrijk, Belgium

Correspondence: Inge Nelissen (inge.nelissen@vito.be) | Ingrid De Meester (ingrid.demeester@uantwerpen.be)

Received: 2 November 2023 | **Revised:** 3 February 2025 | **Accepted:** 12 February 2025

Funding: This work was supported by the University Research Council (BOF) Antwerp under Grant number 45146 (EVZYM project) and VITO.

Keywords: CD26 | high-sensitivity flow cytometry (HS-FCM) | nafamostat mesylate | prostasomes | SARS- CoV-2 | seminal fluid extracellular vesicles (SF-EVs) | transmembrane serine protease 2 (TMPRSS2)

ABSTRACT

Human transmembrane serine protease 2 (TMPRSS2) has garnered substantial interest due to its clinical significance in various pathologies, notably its pivotal role in viral entry into host cells. The development of effective strategies to target TMPRSS2 is a current area of intense research and necessitates a consistent source of active TMPRSS2 with sufficient stability. Here, we comprehensively characterised human seminal-fluid extracellular vesicles (SF-EVs, also referred to as prostasomes), bearing a native source of surface-exposed, enzymatically active TMPRSS2 as demonstrated by high-sensitivity flow cytometry and a fluorometric activity assay. Additionally, we recombinantly produced human TMPRSS2 ectodomain in mammalian cells adopting a directed activation strategy. We observed comparable catalytic parameters and inhibition characteristics for both native SF-EV-associated and recombinant TMPRSS2 when exposed to serine protease inhibitor Nafamostat mesylate. Leveraging these findings, we developed a robust *in vitro* biochemical assay based on these SF-EVs for the screening of TMPRSS2-targeting compounds. Our results will accelerate the discovery and advancement of efficacious therapeutic approaches targeting TMPRSS2 and propel further exploration into the biological role of SF-EV-associated active TMPRSS2.

1 | Introduction

Transmembrane serine protease 2 (TMPRSS2, 54 kDa) belongs to the type II transmembrane serine protease (TTSP) family that comprises four subfamilies of trypsin-like serine proteases (Bugge et al. 2009). Human TMPRSS2 consists of 492 amino acids and

encompasses an N-terminal intracellular domain, a single-pass transmembrane domain, the typical TTSP stem region comprising low-density lipoprotein (LDL) receptor class A (LDLR-A) and scavenger receptor cysteine-rich (SRCR) domains, and a C-terminal peptidase S1 domain (Figure 1) (Paoloni-Giacobino et al. 1997). Similar to other TTSPs, TMPRSS2 is expressed as

This is an open access article under the terms of the [Creative Commons Attribution-NonCommercial-NoDerivs](https://creativecommons.org/licenses/by-nc-nd/4.0/) License, which permits use and distribution in any medium, provided the original work is properly cited, the use is non-commercial and no modifications or adaptations are made.

© 2025 The Author(s). *Journal of Extracellular Vesicles* published by Wiley Periodicals, LLC on behalf of the International Society for Extracellular Vesicles.

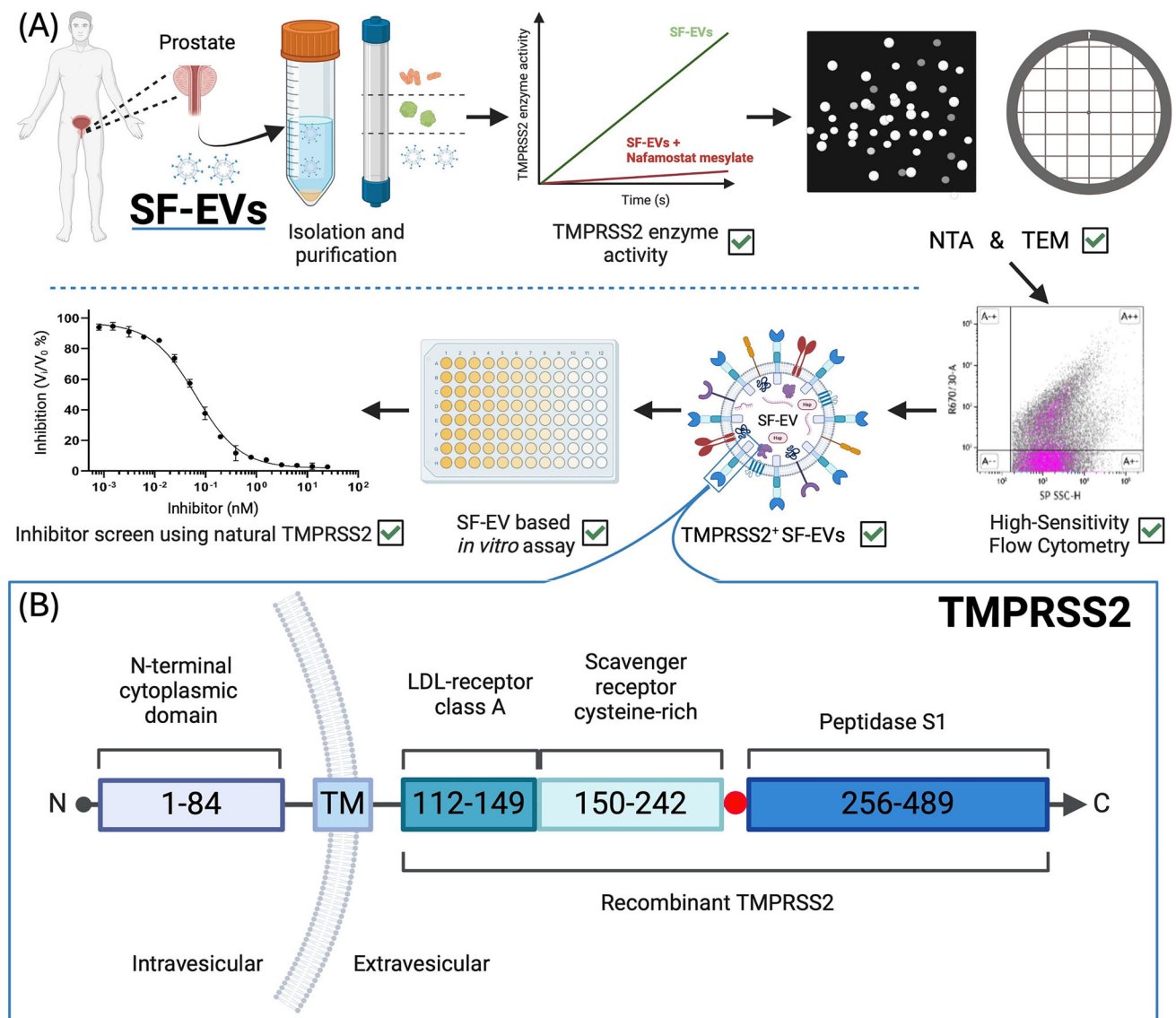


FIGURE 1 | (A) Graphical overview of the experimental set-up, starting with the isolation of seminal fluid extracellular vesicles (SF-EVs) from leftover semen samples via ultracentrifugation and size-exclusion chromatography. The purified SF-EV stocks showed distinctive TMPRSS2 enzyme activity and were characterised for size distribution via nanoparticle tracking analysis (NTA) and transmission electron microscopy (TEM). Then, we confirmed surface-exposed TMPRSS2 on the SF-EVs via high-sensitivity flow cytometry, triggering us to develop an SF-EV based *in vitro* screening assay for TMPRSS2-inhibitors. (B) Architecture of TMPRSS2. Native TMPRSS2 constitutes the N-terminal cytoplasmic, the transmembrane, the LDL-receptor class A, the scavenger receptor cysteine-rich and the peptidase S1 domains. The recombinant TMPRSS2 (dasTMPRSS2, 44 kDa) constitutes the LDL-receptor class A, the scavenger receptor cysteine-rich, the peptidase S1 domain (26 kDa) and an AviTag and C-terminal 8xHIS-tag (not shown), with the enterokinase-cleavable sequence DDDDK²⁵⁵ at the red dot replacing the native SRQSR²⁵⁵ amino acid sequence. TM: transmembrane domain (amino acids 85–105); N and C: N- and C-terminus, respectively. Numbers indicate amino acid position according to UniProt O15393. Figure created with BioRender.com.

single-chain proenzyme (zymogen) that undergoes autoproteolytic cleavage at the interface of the SRCR- and peptidase S1 domain (Arg²⁵⁵↓Ile²⁵⁶) to acquire proteolytic activity (Afar et al. 2001). The peptidase S1 domain (26 kDa) containing the catalytic triad remains linked to the prodomain via an interdomain disulfide bond (Cys²⁴⁴-Cys³⁶⁵). Shedding from the cell membrane has also been documented, although it is unclear whether this occurs under the form of an independent protein entity or as part of an extracellular vesicle (EV) (Afar et al. 2001). Similar to its auto-activation, TMPRSS2 catalyses the hydrolysis of several substrates following a basic amino acid residue (e.g., Arg, Lys), generally

known as ‘trypsin-like’ enzymatic activity (Paoloni-Giacobino et al. 1997; Thunders and Delahunt 2020).

Major TMPRSS2 protein expression is found in the kidneys, gastrointestinal tract (Gkogkou et al. 2020), throughout the upper and lower respiratory system in type II lung alveolar epithelial cells (Donaldson et al. 2002; Bertram et al. 2012; Lukassen et al. 2020; Sarker et al. 2021) and in the lumen and at the apical surface of the prostate secretory epithelium (Afar et al. 2001). Expression can be induced by androgens and some pro-inflammatory conditions (i.e., obesity, autoimmune diseases),

while it can be suppressed by anti-androgen treatment and prostate castration (Gkogkou et al. 2020). TMPRSS2 has been identified in numerous proteomics studies as being present in prostasomes or ‘seminal fluid-derived extracellular vesicles’ (SF-EVs), and its transmembrane structure suggests it is likely to be inserted into the vesicular membrane (Utleg et al. 2003; Zhang et al. 2020; Manouchehri Doulabi et al. 2022; Yang et al. 2017). SF-EVs, akin to other EVs, possess an exceptionally large interactive surface area, facilitating interactions with both cells and molecules within the extracellular microenvironment (Buzás et al. 2018). The term ‘SF-EV’ refers to all EVs released by the male reproductive tract (epithelial cells of the testis, epididymis, ampulla of ductus deferens and accessory sex glands) while the term ‘prostasomes’ theoretically only refers to those EVs originating from the acinar prostate epithelial cells (Roca et al. 2022). Both designations are used interchangeably.

SF-EVs measure about 150 nm in diameter, are partitioned through apocrine exocytosis of multivesicular bodies (Dubois et al. 2015; Ronquist 2012; Ronquist and Brody 1985; Sahlén et al. 2002), and can be secreted by healthy, early-differentiated and cancerous prostate epithelial cells (Lucas et al. 2014; Vaarala et al. 2001; Vaarala et al. 2001). They constitute a distinct bilayered membrane containing lipid rafts, with a dominant contribution of cholesterol and the phospholipid sphingomyelin over phosphatidylcholine (Skotland et al. 2019; Arienti et al. 1998; Arvidson et al. 1989). These lipids foster fluent release of the intraluminal vesicles into the extracellular space of the prostate ducts, into the seminal plasma (Ronquist and Brody 1985; Trajkovic et al. 2008; Brody et al. 1983). The role of SF-EVs as intercellular signalling agents between the immobile acinar cells of the prostate gland and the mobile spermatozoa is widely accepted (Buzás et al. 2018; Ronquist 2012; Pons-Rejraji et al. 2011). As such, SF-EVs (i) activate sperm by releasing acrosome-stimulating enzymes that enhance the motility and fertilizing ability of sperm (Pons-Rejraji et al. 2011; Siciliano et al. 2008; Palmerini et al. 2003; Stegmayr and Ronquist 1982), (ii) modulate the immune response in the host and/or in the female reproductive tract (Kelly et al. 1991; Rooney et al. 1993; Kelly 1995), (iii) protect the male reproductive system via antimicrobial and antiviral strategies (Carlsson et al. 2000; Kitamura et al. 1995) and (iv) stimulate the liquefaction of semen (Lilja and Laurell 1984). Similar to other EV types, they are also credited with a possible utility as markers of disease (Buzás et al. 2018; Kelly 1995; Tanase et al. 2017; Park et al. 2016; Vickram et al. 2020; Duijvesz et al. 2011). Typical SF-EV markers described in the literature include CD10, CD13, dipeptidyl peptidase IV (CD26) and CD59 (Rooney et al. 1993; Kelly 1995; Carlsson et al. 2006; Renneberg et al. 2001; Arienti et al. 1997; Troisi et al. 2023).

Although the physiological role of TMPRSS2 remains largely unknown, TMPRSS2 as part of the SF-EV surface interactome may serve as a receptor, conducting external signalling or interacting with the extracellular matrix through its extracellular protein binding domains (Buzás et al. 2018; Chen et al. 2010). Also, TMPRSS2^{-/-} mice are essentially phenotypically normal (Kim et al. 2006). The enzyme has been proposed to be involved in the progression and metastasis of androgen-dependent prostate cancer due to (i) identification of additional substrates such as TTSP matriptase and hepatocyte growth factor, (ii) the high prostatic expression of TMPRSS2 and (iii) an androgen response element in the 5′ untranslated region of the TMPRSS2 gene (Lin

et al. 1999; Ko et al. 2015; Pawar et al. 2019; Jacquinet et al. 2001; Wilson et al. 2005). Active TMPRSS2 also primes glycoproteins of several viruses (Böttcher et al. 2006; Shirogane et al. 2008; Bertram et al. 2010; Abe et al. 2013; Sakai et al. 2014; Esumi et al. 2015; Saunders et al. 2023; Bestle et al. 2021), including the severe acute respiratory syndrome coronavirus (SARS-CoV) (Glowacka et al. 2011; Matsuyama et al. 2010), the Middle East respiratory syndrome CoV (Shirato et al. 2013; Kleine-Weber et al. 2018), and SARS-CoV-2 (Zang et al. 2020; Hoffmann, Kleine-Weber, Schroeder et al. 2020; Bestle et al. 2020; Li et al. 2021). TMPRSS2 plays a prominent role in the viral entry of SARS-CoV-2 particles through proteolytic cleavage (‘priming’) of the CoV spike protein at the canonical multibasic S1/S2 site, which enables fusion of the viral and cellular membranes (Clausen et al. 2020; Daly et al. 2020; Schneider et al. 2021; Wang et al. 2021; Wei et al. 2021; Wang et al. 2013; Hoffmann, Kleine-Weber, Schroeder et al. 2020; Hoffmann, Kleine-Weber and Pöhlmann 2020). Repeatedly, TMPRSS2 has been shown to be a promising therapeutic target for SARS-CoV-2 as enzyme inhibition leads to a reduced host cell entry (Thunders and Delahunt 2020; Hoffmann, Kleine-Weber, Schroeder et al. 2020; Wettstein et al. 2022).

Development of TMPRSS2-targeting drugs has long been hampered by cumbersome recombinant production of sufficiently stable, active TMPRSS2 from mammalian origin. Only recently, Fraser et al. successfully produced and purified human TMPRSS2 from Sf9 insect cells (Fraser et al. 2022). The scarcity of human recombinant TMPRSS2 (rTMPRSS2) had urged us to search for alternative, biological sources of TMPRSS2. SF-EVs are known to accommodate native TMPRSS2, however it is unknown whether it is enzymatically active and where it is located (Utleg et al. 2003; Zhang et al. 2020; Manouchehri Doulabi et al. 2022; Chen et al. 2010). Provided TMPRSS2 is active within a naturally membrane-bound setting, these SF-EVs present promising prospects for leveraging them in drug development (Laporte and Naesens 2017).

Here we demonstrate that human SF-EVs harbour surface-exposed, enzymatically active TMPRSS2, which enabled us to develop an *in vitro* biochemical assay for the screening of TMPRSS2-targeting compounds (Figure 1). We produced rTMPRSS2 with excellent specific enzymatic activity, by adopting the directed activation strategy from Fraser et al. to a mammalian expression system (Fraser et al. 2022). The rTMPRSS2 was utilised to confirm the suitability of SF-EVs for assessing specific TMPRSS2 inhibition, which was validated using the Lys/Arg-specific serine protease inhibitor Nafamostat mesylate. Leveraging this discovery, we developed an *in vitro* biochemical assay for screening TMPRSS2-targeting compounds with SF-EVs. Our research sets the stage for forthcoming basic and translational investigations into SF-EVs in general and SF-EV-associated TMPRSS2 in particular.

2 | Methods

2.1 | Isolation of Seminal Fluid-Derived Extracellular Vesicles

All the human semen samples were anonymous leftovers collected from fertility clinics between the years 2000 and 2016 (storage at −20°C), donated by healthy volunteers from whom

informed consent was obtained according to the declaration of Helsinki and the internal guidelines of our university (De Bruyn n.d.). Seminal fluid-derived extracellular vesicles (SF-EVs) were isolated from pooled semen samples of at least 50 donors via ultracentrifugation and size-exclusion chromatography, using a protocol described before (Carlsson et al. 2003; De Meester et al. 1996). Samples were thawed at 4°C, pooled, and centrifuged for 10 min at 900 × g to pellet the spermatozoa. The supernatant was collected and centrifuged for 10 min at 2000 × g to pellet dead cells. Then, the retained supernatant was centrifuged for 30 min at 10,000 × g to remove cellular debris. Subsequently, the resulting supernatant was ultracentrifuged for 120 min at 100,500 × g (Optima XPN-100 Ultracentrifuge, Beckman Coulter, California) to pellet the SF-EVs. Finally, SF-EVs were washed with 20 mM Tris-HCl (pH 7.4) and resuspended in the same buffer (De Bruyn n.d.).

The obtained SF-EV suspension was loaded on a HiLoad 16/600 Superdex 200 prep grade column (Figure S1) equilibrated with 20 mM Tris-HCl (pH 7.4). To detect fractions with CD26 enzymatic activity, representative of the SF-EVs, 10 µL elution fraction was mixed with 0.5 mM glycyl-prolyl-para-nitroanilide (Gly-Pro-pNA, Sigma, Cat. No. G0513) substrate in 50 mM Tris-HCl (pH 8.3) in a final volume of 100 µL. CD26 enzyme activity was kinetically determined during 10 min at 37°C in duplicate in a 96-well plate (final volume: 50 µL) by measuring the velocities of pNA release (405 nm) from the chromogenic substrate on an M200 multi-plate reader (Tecan, Männedorf) (Dubois et al. 2008; Matheeußen et al. 2012). The collected fractions were centrifuged for 145 min at 200,000 × g (Optima Max-XP, Beckman Coulter, California) to obtain pure SF-EV pellets, that were resuspended in 20 mM Tris-HCl (pH 7.4) and stored at -80°C until further use (De Bruyn n.d.).

2.2 | Nanoparticle Tracking Analysis (NTA)

This method utilizes the properties of light scattering or fluorescence in combination with Brownian motion in order to obtain the particle size distribution of samples in liquid suspension (Dragovic et al. 2011). Scatter- and fluorescence-based NTA was performed on a ZetaView PMX-220 TWIN instrument (Particle Metrix GmbH, Inning am Ammersee) equipped with a 488 nm laser. The instrument was verified with 100 nm FluoSphere Carboxylate-modified polystyrene beads (Thermo Fisher Scientific, Cat. No. F8803), freshly diluted 1:250,000 in ultrapure water. Purified SF-EVs were diluted 1:100,000 in 20 mM Tris-HCl buffer (pH 7.4). For fluorescent detection, 9 µL diluted SF-EVs were labelled with the membrane-intercalating dye cell mask green (CMG, Thermo Fisher Scientific, Cat. No. C37608) by adding 2 µL CMG (5 mg/mL stock solution in DMSO diluted 1:100 in phosphate-buffered saline [PBS]) and incubation at room temperature (20°C–25°C) for 1 h in the dark. After incubation, the mixture was further diluted to at least 1 mL with ultrapure water to obtain valid recordings with a number of particles per frame between 50 and 200. Next, each sample was measured in technical triplicate at 11 positions in scatter and fluorescence mode with low-bleach function on, shutter set at 100 and sensitivity at 97 (sensitivity 80 in scatter mode). Using the ZetaView software (v8.05.11 SP2) the particle number concentration was calculated, whereas the mean and median diameter and mode were determined from the particle number size distribution.

2.3 | Transmission Electron Microscopy (TEM)

Thawed SF-EV stocks were vortexed and 20 µL of the sample was brought in triplicate on formvar nickel electron microscopy slot grids (Electron Microscopy Sciences, Cat. No. FF2010-Ni-50) and let to adhere for 60 min. The grids were washed two times with PBS, followed by three washes with ultrapure water. Then, the sample was fixed onto the grid with a 2.5% glutaraldehyde solution for 10 min, after which the grids were washed again twice with ultrapure water. The sample was contrasted with a 2% uranyl acetate solution for 15 min and embedded in a 0.13% methylcellulose and 0.4% uranyl acetate solution for 10 min. The samples were dried and visualized in a Tecnai G2 Spirit Bio TWIN microscope (Thermo Fisher Scientific, Eindhoven, The Netherlands) at 120 kV.

2.4 | SF-EV Protein Isolation and Quantification

Freshly purified SF-EV fractions or prostate cancer cells (PC3) were lysed in an appropriate volume of 1% octyl glucoside (120 mM NaCl, 50 mM Tris-HCl, pH 8.0) on ice for 1 h with thorough vortexing every 15 min, followed by centrifugation for 10 min at 12,000 × g. The protein content in the supernatant was assessed according to the method of Bradford et al. using bovine serum albumin (BSA, Thermo Fisher Scientific, Cat. No. 240401000) as a standard. A total of 10 µL of sample was added to a 96-well microplate followed by 100 µL of Bradford reagent (Bradford 1976). The absorbance was measured at 595 nm (Molecular Devices, SpectraMax Plus 384, SoftMax Pro v7.0.3. software) and protein concentration was determined from the BSA standard curve. Result is presented as the mean ± s.d. of three independent measurements.

2.5 | Recombinant TMPRSS2 Protein Production

2.5.1 | Construct Design and Cloning

A construct encoding residues 109–492 comprising soluble ‘directed activation strategy TMPRSS2’ (Fraser et al. 2022) was ordered from Genscript. It constitutes the LDL-receptor class A, the scavenger receptor cysteine-rich and the peptidase S1 domains. The final construct contained an N-terminal µ-phosphatase secretion leader peptide (MGILPSPGMPALLSLVLSVLLMGCVAE), a C-terminal AviTag and 8xHis-tag, and the enteropeptidase-cleavable DDDDK²⁵⁵ site, which replaced the natural SRQSR²⁵⁵ graft to allow on-demand activation of the pro-enzyme using enterokinase. Our engineered TMPRSS2 protein expression construct is available on Addgene (plasmid no. 207850). The plasmid transfer vector containing the TMPRSS2 gene (aa 109–492) was transformed into *Escherichia coli* TOP10F’ cells (Thermo Fisher Scientific, Cat. No. C303003) to amplify recombinant plasmid DNA, and the Plasmid Maxi Kit (Qiagen, Cat. No. 12163) was used to isolate the plasmid DNA.

2.5.2 | TMPRSS2 Protein Production in Freestyle 293-F Cells

Freestyle 293-F cells (Thermo Fisher Scientific, Cat. No. R79007) were cultured in Freestyle 293 medium (Thermo Fisher Scientific,

Cat. No. 12338018) on an orbital shaker (117 rpm, 37°C, 5% CO₂), for at least three passages. The cells were transfected chemically at a density of $\pm 1 \times 10^6$ cells per mL with 1 µg plasmid DNA and 3 µg polyethylenimine (Merck, Cat. No. 408727) per mL of cell culture.

2.5.3 | TMPRSS2 Protein Purification and Zymogen Activation

Cell culture medium containing the final secreted protein product TMPRSS2(109-492)-GS-AviTag-8xHIS (44 kDa) was collected by double centrifugation (5 min, 4°C, 1000 × g; 20 min, 4°C, 18,000 × g) approximately 4 days post-transfection when cell viability dropped to 75%. The centrifuged medium was filtered through a 0.22 µm filter and adjusted to pH 7.2 by addition of concentrated HEPES buffer (250 mM HEPES, 1.5 M NaCl, pH 7.2) in a 1:10 ratio, before loading the buffered cell culture medium onto a HisTrap excel column (Cytiva, Cat. No. 17371206) equilibrated with equilibration buffer (25 mM HEPES, 150 mM NaCl, pH 7.2). The protein was isocratically eluted with equilibration buffer supplemented with 250 mM imidazole (Figure S4A). Elution samples were pooled, slightly concentrated in a Vivaspin 20 centrifugal concentrator (Sartorius, Cat. No. VS2001) to a volume <3 mL and subsequently loaded onto a HiLoad 16/600 Superdex 75 pg column (Cytiva, Cat. No. 28989333) for size-exclusion chromatography in a buffer composed of 50 mM Tris, 150 mM NaCl, pH 7.5 (Figure S4B). The elution fractions containing TMPRSS2 were then detected via dot blotting (Supporting Information Method 1; Figure S4C), using in-house purified HIS-tagged ICAM-1 as positive control, and SDS-PAGE analysis (Figure S4D). The samples were concentrated to a protein concentration of 1 mg/mL and buffer exchanged via centrifugation (Amicon Ultra 0.5mL—Ultracel 10K, Merck Millipore Cat. No. UFC501024) to 20 mM Tris-HCl, 50 mM NaCl, 2 mM CaCl₂, pH 8. The purified protein sample was divided into 49 µL aliquots, to which 1 µL enterokinase (16,000 U/mL, New England Biolabs, Cat. No. P8070) was added for overnight TMPRSS2 zymogen activation in the dark at 16°C. To remove enterokinase, the activated TMPRSS2 was subjected to size-exclusion chromatography using an ENrich SEC 70 column (Bio-Rad, Cat. No. 780-1070), in a buffer composed of 50 mM sodium phosphate, 250 mM NaCl, 1% glycerol, pH 6 (Figure S4E). Pure elution fractions containing TMPRSS2 were detected via dot blotting (Supporting Information Method 1; Figure S4F), collected, confirmed by western blotting (Figure S4G) and stored at -80°C in the same buffer.

2.6 | Enzyme Activity Assays

2.6.1 | Trypsin-Like Enzyme Activity Assay

Trypsin-like enzymatic activity of the intact SF-EVs (final concentration in well: 3.3×10^{10} vesicles/mL) or recombinant TMPRSS2 (rTMPRSS2; final concentration in well: 50 pM) was determined using 100 µM generic TTSP fluorogenic peptide derivative N-tert-butoxycarbonyl-Gln-Ala-Arg-7-amino-4-methylcoumarin (Boc-QAR-AMC; 50 mM Tris, 120 mM NaCl, pH 8.0) (Bachem, Cat. No. 4017019). This substrate is rapidly cleaved by active TMPRSS2, C-terminal to Arg, thereby releasing fluorescent 7-amino-4-methylcoumarin (AMC) product and enabling initial reaction velocity (V_0) measurement. SF-EVs or enzymes were preincubated for 15 min at 37°C with either

vehicle (1% DMSO) or with 1 µM in-house synthesised inhibitor N-(1H-indazol-3-yl)quinoline-4-amine (Laboratory of Medicinal Chemistry, University of Antwerp). The specific trypsin-like enzyme activity is defined as the difference in initial reaction velocity (V_0) between enzyme with or without inhibitor. Fluorescence was kinetically measured for 20 min at 37°C in a half-area 96-well plate (Greiner Bio-One, Cat. No. 675101) (final volume: 50 µL) on an F200 multi-plate reader (excitation: 380 nm, emission: 460 nm) (Tecan, Männedorf, Switzerland) using the Magellan software (v7.2).

2.6.2 | Determination of Michaelis-Menten Kinetics

The apparent Michaelis constant (K_m , Supporting Information Equation 1) of SF-EVs and rTMPRSS2 for the substrate Boc-QAR-AMC was determined by adding pre-warmed SF-EVs (final concentration in well: 3.3×10^{10} vesicles/mL) or rTMPRSS2 (final concentration in well: 50 pM) to pre-warmed Boc-QAR-AMC (7 concentrations from 15 to 1000 µM) in duplicate. Substrate conversion was kinetically measured over 20 min at 37°C in a half-area 96-well plate (final volume: 50 µL). Initial reaction velocities (V_0) were plotted against substrate concentration and curve fitted using GraphPad Prism (v9.1.1). Initial reaction velocities (RFU/min) were normalised using an AMC calibration curve (0.3–10 µM) to µmol/L/min and plotted against the substrate concentrations using GraphPad Prism. K_m values are presented as the mean \pm s.d. of three independent assays on SF-EV preparations from separate pools ($n = 3$), each performed in technical duplicate.

2.6.3 | IC₅₀ Measurement

The half-maximal inhibitory concentration (IC₅₀, Supporting Information Equation 2) of Nafamostat mesylate (Selleckchem, also named FUT-175, Cas No. 82956-11-4) was determined by pre-incubating SF-EVs (final concentration in well: 3.3×10^{10} vesicles/mL) or rTMPRSS2 (final concentration in well: 50 pM) with inhibitor (12 concentrations ranging from 0.14 pM to 25 nM) in duplicate for 15 min at 37°C in a half-area 96 well plate. Pre-warmed Boc-QAR-AMC was added in a final concentration of 100 µM. Initial reaction velocities were kinetically measured at 37°C in a 96 well plate (final volume: 50 µL). IC₅₀ values were determined after generating a nonlinear regression analysis from a plot of fractional enzyme activity (V_i/V_0) versus [Inhibitor] using GraphPad Prism (v9.1.1). IC₅₀ values are presented as the mean \pm s.d. of three independent assays on SF-EV preparations from separate pools ($n = 3$), each performed in technical duplicate.

2.7 | High-Sensitivity Flow Cytometry (HS-FCM)

2.7.1 | Antibody Staining of SF-EVs

SF-EVs were diluted in PBS pH 7.2 (Life Technologies, Cat. No. 20012-09) down to a concentration of 1.25×10^{10} SF-EVs per mL. SF-EV samples as well as background control samples (PBS) were fluorescently stained with 10 µM Vybrant CFDA-SE (Thermo Fisher Scientific, Cat. No. V12883) as previously described (Groot Kormelink et al. 2016). Next, these samples (100 µL) were stained with either mouse anti-human CD26-APC (2.4 µg/mL), mouse

anti-human TMPRSS2-APC (11 µg/mL) or the corresponding IgG isotype control antibodies (equal amount per sample; Table S3). Antibodies were centrifuged (17,000 × g, 5 min, 4°C) before use to remove aggregates. The optimal staining concentrations of the antibodies were determined by titration according to Welsh et al. (data not shown) (Welsh et al. 2023). Besides measuring the presence of the TMPRSS2 and CD26 marker, isotype controls were analysed for determining non-specific binding (Figures S13 and S14). Stained SF-EVs were further purified overnight by bottom-up density gradient centrifugation using a iodixanol gradient (OptiPrep, StemCELL Technologies, Cat. No. 07820). A bottom-up iodixanol gradient was prepared as described in Deville et al. (2021). Iodixanol fractions of 480 µL were collected and measured on the flow cytometer to select the fraction containing the most SF-EVs (i.e., fraction 6). From this fraction, 1/50 dilutions were prepared and measured using flow cytometry. For this dilution factor, the absence of swarming was confirmed (Figure S16). Necessary controls (i.e., unstained buffer, stained buffer, unstained sample, isotype controls; Figures S8–S18) were tested. Detergent control measurements were performed by treating isolated and stained SF-EVs with 1% Triton-X100 (Sigma-Aldrich, Cat. No. X100-500ML) in the dark at room temperature (20°C–25°C) for 30 min. The treatment with detergent resulted in a decrease (81%–94%) of the antibody signal.

2.7.2 | Flow Cytometric Analysis of SF-EVs

HS-FCM was performed on a BD FACSymphony A1 Flow Cytometer (BD Biosciences, San Jose, CA, USA) equipped with a 488 nm laser (both 100 mW) and a 637 nm laser (100 mW). SP-SSC signals were collected from the 488 nm laser into a PMT (395–411V), FITC fluorescent signals were collected from the 488 nm laser into a PMT (499–502 V) fitted with a 530/30 bandpass filter and 505 long pass mirror, APC fluorescent signals were collected from the 637 nm laser into a PMT (669–672 V) fitted with a 670/30 bandpass filter and 655 long pass mirror. Before starting QC measurements, the device was rinsed with PBS pH 7.2 (Life Technologies, Cat. No. 20012–019) for 1 h. QC was performed using BD FACSDiva CS&T Research Beads (BD, Cat. No. 655051) and Megamix-Plus SSC (Biocytex, Cat. No. 7803). After QC, the device was rinsed with PBS (5 min), diluted BD Detergent Solution Concentrate (BD, Cat. No. 660585) (10 min), and finally PBS (10 min) at setpoint ‘HIGH’ and ‘80’. Data was acquired for 60 s at setpoint ‘LOW’ and ‘80’. For these settings sample flow rate was determined in the beginning and at the end of each experiment using BD TruCOUNT Control beads (BD, Cat. No. 340335). The mean sample flow rate for each experiment was between 4.0 and 5.1 µL/min. The SP-SSC trigger threshold was set at 200, which we previously tested and demonstrated to be able to measure 100 nm polystyrene beads (data not shown). This setting resulted in the collection of less than 536 events/s in unstained PBS. All samples were measured in technical duplicate or triplicate, on different days. Instruments settings were adjusted and data was recorded in BD FACSDiva (v9.0.2). All data was analysed using Kaluza v 2.1 (Beckman Coulter). Gates were set as described in the MIFlowCyt checklist (Table S5). Designated Molecules of Equivalent Soluble Fluorochrome (MESF) beads (Bangs Laboratories, Quantum APC MESF Cat. No. 823A and Quantum FITC-5 MESF Cat. No. 555A) were used to create a standard curve of geomean fluorescence intensity (MFI) versus

MESF values (Figure S18). Threshold for APC was 720 MESF, threshold for FITC was 71 MESF. Rosetta Calibration beads (Exometry, Cat. No. CAL003) were measured to convert the arbitrary units of the light scattering signal to nanometres.

2.8 | Gel Electrophoresis and Western Blotting

For SDS-PAGE and western blotting of SF-EVs, 3 µg of SF-EV lysate or human PC3 prostate cancer cell lysate, as determined via Bradford protein quantification, were diluted in 4× Laemmli sample buffer (250 mM Tris-HCl (pH 6.8), 8% (w/v) (SDS), 0.2% (w/v) bromophenol blue, 40% (v/v) glycerol, 20% (v/v) β-mercaptoethanol), heated to 95°C for 10 min, loaded onto a 4%–20% Mini-PROTEAN TGX Stain-Free Protein Gel (Bio-Rad, Cat. No. 4568096) and separated at 140 V for 60 min. The proteins were transferred to a 0.45 µm nitrocellulose membrane (Bio-Rad, Cat. No. 1620115) at 250 mA for 60 min. Aspecific binding was blocked by incubation of the blotted membrane in blocking buffer (5% non-fat dried milk powder (VWR, Cat. No. A0830.0500) in freshly made phosphate-buffered saline (PBS; for TMPRSS2 and Calnexin detection) or tris-buffered saline (TBS; for CD26, HSPA8 and β-actin detection) for 60 min at room temperature (20°C–25°C) with gentle shaking. Membranes were then incubated with primary antibody (Table S1) diluted in blocking buffer supplemented with 0.1% Tween-20, overnight at 4°C with gentle shaking. After washing (PBS or TBS supplemented with 0.1% Tween-20 [PBS-T/TBS-T]), membranes were incubated with HRP-conjugated secondary antibody (Table S2) diluted in blocking buffer with 0.1% Tween-20, for 2 h at room temperature (20°C–25°C) with gentle shaking. Antibodies were centrifuged (17,000 × g, 5 min, 4°C) before use to remove aggregates. Finally, membranes were washed (PBS-T/TBS-T) and the bands were visualised by adding SuperSignal West Femto Maximum Sensitivity Substrate (Life Technologies, Cat. No. 34096) for 60 s, and analysed by a Molecular Imager ChemiDoc MP imaging system using the Image Lab v6.1 software (BioRad Laboratories, Hercules, CA, USA).

For rTMPRSS2 gel electrophoresis, SDS-PAGE was carried out as described, with 10 µL size-exclusion chromatography elution fraction or 25 ng purified TMPRSS2 diluted in 4× Laemmli sample buffer. For visualisation of the separated proteins, the gel was incubated with Oriole fluorescent gel stain for 90 min in the dark, and imaged using the Molecular Imager ChemiDoc MP imaging system and the Image Lab v6.1 software (BioRad Laboratories, Hercules, CA, USA). For western blotting, a similar protocol was used as described before (SDS-PAGE and Western blotting of SF-EVs), using the anti-HIS-tag primary antibody (Table S1), PBS-T as washing buffer and PBS supplemented with 5% non-fat dried milk powder as blocking buffer.

2.9 | SF-EV-Based In Vitro Screening Assay for TMPRSS2-Targeting Compounds

2.9.1 | Optimization of Assay

To optimize an in vitro assay for screening of TMPRSS2-targeting compounds, SF-EVs and substrate were combined at various concentrations. Nafamostat mesylate was included as a reference

inhibitor in each experiment at a final concentration of 100 nM. SF-EVs were incubated with the reference inhibitor or buffer for 15 min at 37°C. Afterwards, Boc-QAR-AMC was added, and fluorescence was measured for 60 min on an F200 multi-plate reader (excitation: 380 nm, emission: 460 nm) (Tecan, Männedorf, Switzerland) using the Magellan software (v7.2). In the first experiment, reagents were combined in a half-area 96-well plate in an end volume of 60 µL. The vesicle concentration varied from 7.2×10^9 to 1.8×10^{10} vesicles/mL, using 5, 10 or 15 µM as the substrate concentration. This experiment was repeated in a black 384-well plate (Greiner Bio-One, Cat. No. 781079) with SF-EV concentrations varying from 1.4×10^9 to 1.4×10^{10} vesicles/mL, identical substrate concentrations and in an end volume of 40 or 20 µL. The following parameters were evaluated: (i) specific trypsin-like enzyme activity, (ii) substrate conversion where the total amount of consumed substrate should be kept below 10% to avoid saturation of the target protease and substrate depletion, (iii) signal to blank ratio (S/B) should be at least 10 for accurate quantitative analysis and (iv) Z factor (Z'), a measure to quantify the suitability of a particular assay for full-scale high-throughput screening. Z factor should be above 0.6 with an ideal assay achieving a Z factor of 1 (Supporting Information Equation 3). These parameters guided the selection of optimal vesicle and substrate concentrations to meet the assay requirements of the European Lead Factory (ELF) (Table S6).

2.9.2 | Verification of assay robustness

As a measure of assay robustness, the influence of methanol and DMSO was studied. SF-EVs (7.2×10^9 vesicles/mL) were incubated with methanol or DMSO for 15 min at 37°C. The final methanol and DMSO concentrations varied between 0% and 2.5%. Boc-QAR-AMC was added in a final concentration of 15 µM and fluorescence was kinetically measured at 37°C for 60 min in a black 384-well plate (final volume: 40 µL). Enzyme activity was compared between the wells with or without methanol or DMSO respectively to determine the effect of the solvent. Furthermore, the influence of temperature during incubation and measurement was evaluated. SF-EVs (7.2×10^9 vesicles/mL) were incubated with inhibitor or buffer for 15 min at 37°C or room temperature (20°C–25°C) before adding Boc-QAR-AMC to a final concentration of 15 µM. Fluorescence was kinetically measured at 37°C for 60 min in a black 384 well plate (final volume: 40 µL). Finally, the coefficient of variation (CV) was calculated for different batches within and between days. All batches were equally diluted to a vesicle concentration of 7.2×10^9 vesicles/mL and fluorescence was kinetically measured at 37°C for 60 min in a black 384 well plate (final volume: 40 µL). This experiment was repeated three times in 1 day and on three different days. CVs for repeatability (between run) and intermediate precision (between day) experiments were calculated based on the enzyme activity.

2.10 | Data Management

Data on SF-EVs were reported according to the MISEV guidelines and all the relevant data of our experiments were submitted to the EV-TRACK knowledge base (ID: EV231002) (Théry et al. 2018; Van Deun et al. 2017). Flow cytometry raw data files (.fcs) have been uploaded to FlowRepository (ID: FR-FCM-Z7YY).

3 | Results

3.1 | SF-EVs Contain Enzymatically Active, Surface-Exposed TMPRSS2

Samples of SF-EVs, isolated and purified from pooled-donor liquified semen samples by a combination of (ultra)centrifugation and size-exclusion chromatography (Figure S1), were first subjected to nanoparticle tracking analysis (NTA). The purified SF-EV preparations constituted a heterogeneous group of vesicles between 50 and 400 nm with a median diameter of 140.4 nm in light scatter mode (LS-NTA) or 151.6 nm in fluorescence mode (F-NTA). Based on the mean particle concentration obtained using F-NTA (6.6×10^{14} vesicles/mL) versus LS-NTA (4.6×10^{15} vesicles/mL), about 14.3% of all detected particles were identified as putative SF-EVs (Figure 2A; $n = 3$), similar to earlier findings (Midekessa et al. 2021). These findings could also be confirmed with transmission-electron microscopy (TEM; Figures 2B,C and S3) (Dubois et al. 2015; Ronquist 2012; Ronquist and Brody 1985; Poliakov et al. 2009). The protein content of the SF-EV preparations measured 31 ± 4 g/L, which corresponded to a particle-to-protein ratio around $2.1 \pm 0.2 \times 10^{10}$ particles/µg protein.

In the purified SF-EVs samples a high and very stable trypsin-like activity (± 300 µmol/L/min; undiluted) was measured, which remained stable for up to 1 week at 4°C and minimally 6 months at –80°C, and was not influenced by at least five freeze-thaw cycles (Supporting Information Method 2; Figure S2B). Size-exclusion chromatography confirmed that ~99% of the trypsin-like enzyme activity originated from vesicle-bound TMPRSS2. A new ultracentrifugation step of previously purified SF-EV stocks upon thawing, resulted in $30\% \pm 3\%$ detachment of TMPRSS2 from SF-EVs ($n = 2$). To obtain the apparent K_m of the SF-EVs with the fluorogenic substrate Boc-QAR-AMC, the initial reaction velocity (V_0) was plotted against the substrate concentration and fitted with the Michaelis-Menten equation (Figure 3A; $n = 3$). The apparent K_m for SF-EVs with Boc-QAR-AMC measured 278 ± 52 µM and the V_{max} equalled 4.71 ± 0.35 µmol/L/min. Additionally, the potency of Nafamostat mesylate was investigated, an inhibitor which forms a slowly reversible covalent complex with the catalytic serine residue of trypsin-like proteases, and resulted in a half-maximal inhibitory concentration (IC_{50}) of 31 ± 5 pM for the SF-EVs (Figure 3B; $n = 3$).

Screening results obtained with this naturally expressed human TMPRSS2 in a complex molecular environment were confirmed using recombinant TMPRSS2 (rTMPRSS2). Optimisation of the secretion signal, the N-terminal non-coding sequence, the purification tag and glycosylation patterns resulted in the generation of a construct that enabled successful production and purification of a secreted, on-demand activated TMPRSS2 ectodomain zymogen from our Freestyle 293-F cell expression system (Figure S4). Following protein activation with enteropeptidase, we achieved highly active rTMPRSS2. We characterised the purified rTMPRSS2 by measuring several Michaelis-Menten parameters. rTMPRSS2 purified to apparent homogeneity demonstrated a K_m of 133 ± 16 µM for the substrate Boc-QAR-AMC, k_{cat} of 20 ± 1 s and V_{max} of 24.4 ± 1.1 µmol/mg/min enzyme (Figure 3B). To the best of our knowledge, this indicates a similar to improved specific

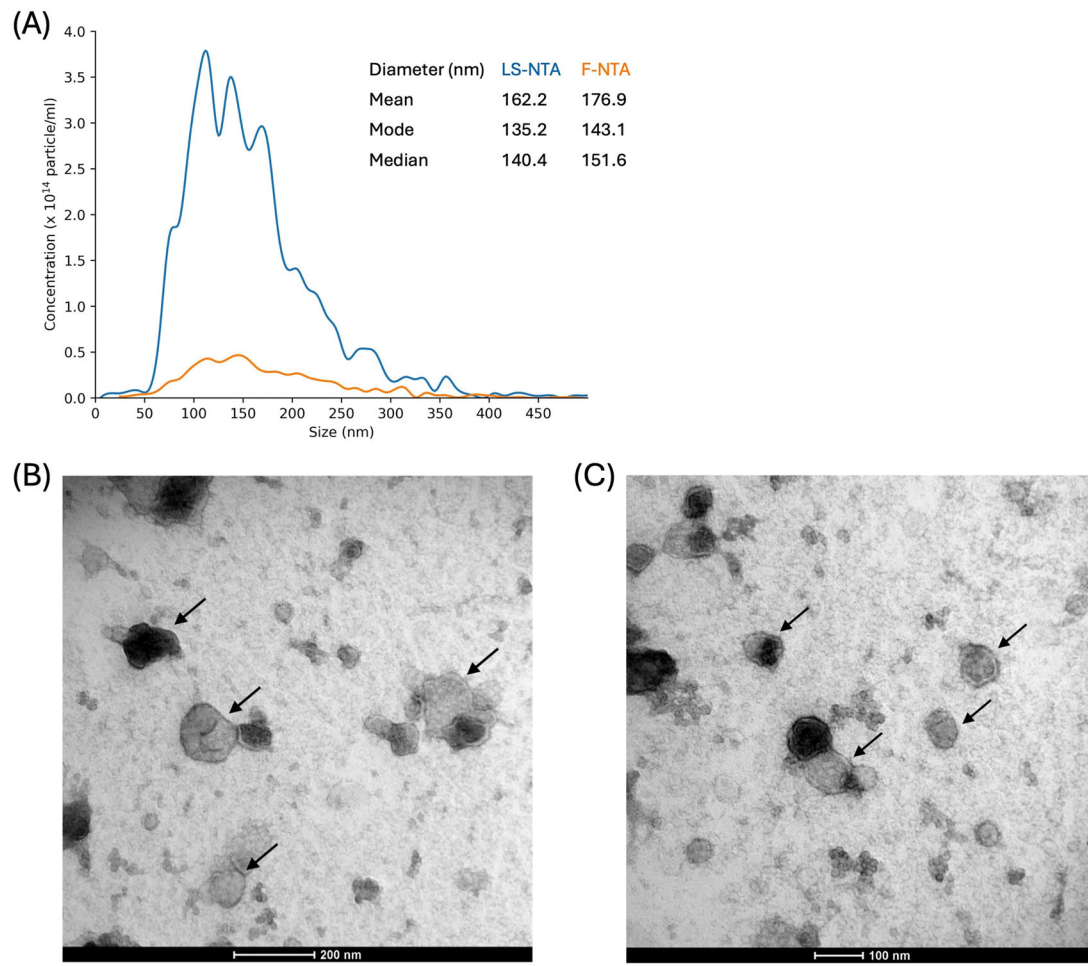


FIGURE 2 | Size, concentration and morphology of SF-EVs by nanoparticle tracking analysis (NTA) and transmission electron microscopy (TEM). (A) Number concentration-based size distribution of SF-EVs in liquid suspension (Tris-HCl) as measured by NTA. The vast majority of SF-EVs are distributed within the size range of 50–400 nm. Legend: Mean, mode and median diameter of SF-EVs measured in light scatter (LS-NTA, blue) and fluorescence (F-NTA, orange) mode are given ($n = 3$). (B and C) SF-EVs as visualised by TEM, example SF-EVs indicated by black arrows. Overview images at lower magnifications can be found in Figure S3A,B, respectively.

enzyme activity compared to previously described rTMPRSS2 preparations (Figure 3C; $n = 3$) (Fraser et al. 2022; Hoffmann et al. 2021; Meyer et al. 2013; Nimishakavi et al. 2015). To assess the functionality of our rTMPRSS2 and to validate our results obtained with the SF-EVs, we determined the IC_{50} for Nafamostat mesylate (Nimishakavi et al. 2015). In our assay, Nafamostat mesylate exhibited high inhibitory potency against rTMPRSS2, with an IC_{50} of 68 ± 3 pM, which corroborated the IC_{50} of Nafamostat mesylate against SF-EVs (Figure 3D; $n = 3$).

3.2 | HS-FCM Confirms SF-EV-Membrane Localisation of TMPRSS2

The activity and inhibition measurements suggested that (auto-)activated TMPRSS2 remains membrane-bound on SF-EVs, enabling their use as a source of active TMPRSS2 in a physiologically relevant format. We exploited high-sensitivity flow cytometry to uncover TMPRSS2 on the SF-EV membrane, in comparison to the well-known SF-EV marker dipeptidyl peptidase 4 (CD26) (Troisi et al. 2023; Vanhoof et al. 1992). SF-EVs pre-stained with CFDA-SE were either incubated with APC-labelled

anti-TMPRSS2 or anti-CD26 antibody. We quantified the fraction of CFDA-SE positive events that showed double positivity for APC staining, as depicted in Figure 4. Following optimisation of the immunostaining and gating conditions (Welsh et al. 2023), $25.5\% \pm 0.7\%$ of CFDA-SE positive events were double positive for TMPRSS2 and $11.3\% \pm 1.5\%$ of CFDA-SE positive events were double positive for CD26 (Figure 4). Upon size calibration of the HS-FCM instrument, we could assign the markers to SF-EVs with a diameter between 100 and 200 nm (Figures S6 and S7), corresponding to the main SF-EV population detected using F-NTA. The respective IgG isotype control antibodies incubated with SF-EVs according to the same procedure gave low to moderate percentage positive events (Table S4; Figures S13 and S14).

Lastly, TMPRSS2 occurrence in the SF-EVs was also demonstrated using western blotting, next to a set of characteristic extracellular vesicle markers, including CD26 (SF-EV-specific), β -actin and HSPA8. The absence of type I integral endoplasmic reticulum membrane protein Calnexin from the SF-EVs was included as a negative control (Figure S5). In SF-EVs, a small amount of intact ‘extracellular’ domain of TMPRSS2 (~44 kDa)

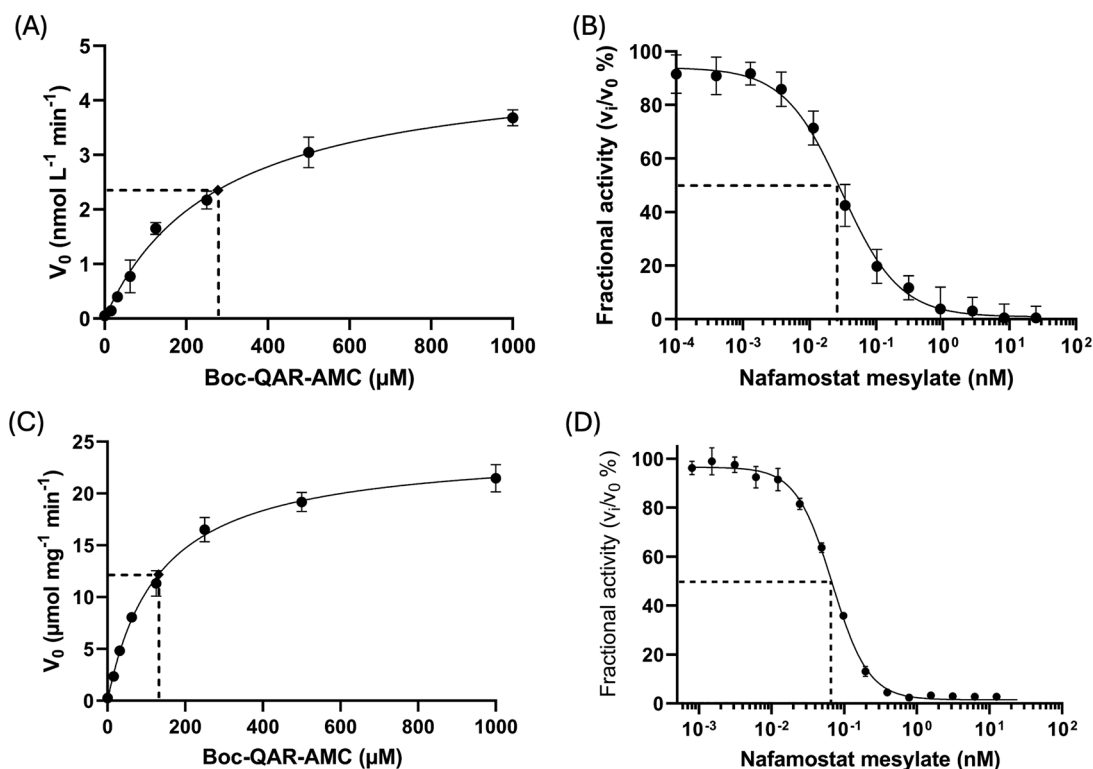


FIGURE 3 | SF-EVs and recombinant TMPRSS2 both display specific trypsin-like enzyme activity. (A) Michaelis–Menten plot of initial reaction velocities (V_0) for kinetic parameter estimation of the generic Boc-QAR-AMC fluorogenic substrate cleaved by SF-EVs ($\pm 3.3 \times 10^{10}$ vesicles/mL), after curve fitting in GraphPad (Supporting Information Equation 1). Michaelis constant (K_m : $278 \pm 52 \mu\text{M}$) is indicated by dotted line. (B) Plot of the fractional enzyme activity in SF-EVs (3.3×10^{10} vesicles/mL) versus [Nafamostat mesylate] by measuring the initial reaction velocities at 37°C in the presence of $100 \mu\text{M}$ Boc-QAR-AMC fluorogenic substrate and curve fitting for absolute IC_{50} determination in GraphPad (Supporting Information Equation 2). IC_{50} ($31 \pm 5 \text{ pM}$) is indicated by dotted line. (C) Michaelis–Menten plot of initial reaction velocities for kinetic parameter estimation of the generic Boc-QAR-AMC fluorogenic substrate cleaved by recombinant TMPRSS2 (50 pM), after curve fitting in GraphPad (Supporting Information Equation 1). Michaelis constant (K_m : $133 \pm 16 \mu\text{M}$) is indicated by dotted line. (D) Plot of the fractional enzyme activity of recombinant TMPRSS2 (50 pM) versus [Nafamostat mesylate] by measuring the initial reaction velocities at 37°C in the presence of $100 \mu\text{M}$ Boc-QAR-AMC fluorogenic substrate and curve fit for absolute IC_{50} in GraphPad (Supporting Information Equation 2). IC_{50} ($68 \pm 3 \text{ pM}$) is indicated by dotted line. All data are shown as mean \pm s.d. and were all performed in biological triplicate ($n = 3$). Graphs were created with GraphPad Prism v9.1.1.

was detected along with a relatively large amount of the smaller catalytic Peptidase S1 domain (26 kDa) (Figure 5) (Zhang et al. 2022).

3.3 | SF-EV-Associated TMPRSS2 Is a Valid, Native Tool for In Vitro Screening of Inhibitory Compounds

These promising results encouraged us to develop an in vitro biochemical screening assay using SF-EVs as an enzyme source for the screening of TMPRSS2-targeting compounds. Different combinations of downscaled vesicle and substrate concentrations were evaluated regarding substrate conversion, coefficient of variation (CV), signal to blank ratio (S/B) and Z factor (Z'). The assay was optimised as to fulfill the requirements for an in vitro screening assay as suggested by the European Lead Factory (ELF), a collaborative public-private partnership that aims to facilitate drug discovery (Table S6). A vesicle concentration of 7.2×10^9 vesicles/mL proved superior as higher vesicle concentrations led to substrate conversion exceeding the accepted limit of 10% (Wu et al. 2003). S/B ratio and Z factor remained optimal for all parameters (Table S7; Figure S19).

In the subsequent stage, the assay underwent miniaturization to 384-well plate format to increase sample throughput, while simultaneously reducing SF-EV concentrations. However, this resulted in insufficient Z' values when employing only $5 \mu\text{M}$ of substrate, while the highest Z factors were achieved using $15 \mu\text{M}$ substrate. Although most conditions met the criteria for a biochemical screening assay, a substrate concentration of $15 \mu\text{M}$ in combination with 7.2×10^9 vesicles/mL was selected for further assay development due to optimal substrate conversion ($6.0\% \pm 0.1\%$), S/B ratio (>100) and Z factor (0.94) (Table S8 and Figure S20). Next, downsizing of the assay volume to 40 or 20 μL was evaluated. While both conditions met the ELF criteria, a 40 μL assay volume was preferred because of a considerably higher Z factor and the less time-consuming, more feasible manual plate preparation in an academic setting without automation (Table S9).

To assess the assay robustness, the temperature during preincubation and measurement was varied. Therefore, the assay was performed at room temperature (20°C – 25°C) and 37°C . Enzyme activity, substrate conversion, S/B-ratio and Z factor did not change between these conditions (Table S10). The effect of the

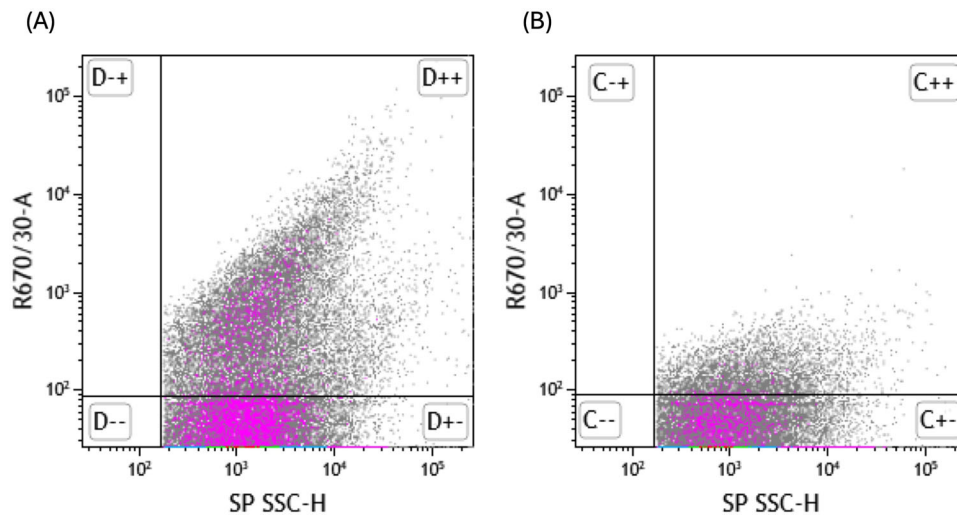


FIGURE 4 | High-sensitivity flow cytometry analysis of SF-EVs. Density plots (R670/30-A vs. SP SSC-H) of purified SF-EVs co-stained with CFDA-SE and (A) anti-human TMPRSS2-APC or (B) anti-human CD26-APC, followed by bottom-up density gradient ultracentrifugation. The plots show a 60 s analysis of fraction 6 (1:50 dilution in PBS) and are representative of technical duplicate or triplicate ($n = 2-3$). All axes are denoted in arbitrary units. Gates were set as described in the MIFlowCyt checklist (Table S5). (A) The density plot of CFDA-SE positive events labelled with anti-human TMPRSS2 antibody demonstrates a moderate increase in the APC signal (R670/30-A). (B) The density plot of CFDA-SE positive events labelled with anti-human CD26 antibody demonstrates a low increase in the APC signal (R670/30-A).

solvents methanol and DMSO on the trypsin-like activity of SF-EVs was examined based on substrate conversion between SF-EVs incubated with methanol or DMSO and SF-EVs without these solvents. No effect on enzyme activity was observed with either DMSO or methanol up to a concentration of 2.5% (one-way ANOVA, p value DMSO: 0.225; p value methanol: 0.154) (Table S11). Lastly, replication of assay performance with multiple SF-EV batches within and between days did not lead to aberrated outcomes on enzyme activity. The coefficient of variation (CV) on enzyme activity was minimal for batches B and C (CV < 10%) and acceptable for batch A (CV < 30%; Tables S12 and S13), while maintaining a stable substrate conversion, S/B ratio and Z factor. Consequently, we demonstrated the suitability of native TMPRSS2 present on SF-EVs to develop a robust in vitro assay for inhibitor screening.

4 | Discussion

The androgen-responsive gene encoding TMPRSS2 is highly expressed in prostate epithelial cells and in human prostate cancers (Afar et al. 2001; Vaarala et al. 2001; Lin et al. 1999). To the best of our knowledge, this is the first description of proteolytically active TMPRSS2 expression on the membrane of SF-EVs, confirmed by combination of an enzyme activity assay and high-sensitivity flow cytometry (HS-FCM). We harnessed the availability of biologically available natural human TMPRSS2 to develop an in vitro biochemical screening assay for TMPRSS2-targeting molecules. Furthermore, we successfully achieved the recombinant expression, purification and characterisation of TMPRSS2 from mammalian origin, essential in validating the specific inhibition of SF-EV-associated TMPRSS2.

Nanoparticle tracking analysis (NTA) of the isolated and purified SF-EV preparations demonstrated a median diameter similar to literature and was confirmed with TEM (Figure S3). However,

it should be noted that smaller vesicles may remain undetected due to the NTA limit of detection for biological nanoparticles of around 50 nm (Dubois et al. 2015; Ronquist 2012; Ronquist and Brody 1985; Poliakov et al. 2009; Bohren and Huffman 2007). A clearly decreased SF-EV count from fluorescent NTA (F-NTA) compared to light-scattering NTA (LS-NTA) has been described before (Hirschberg et al. 2022). Midekessa et al. discovered that SF-EVs exhibited lower labelling efficiency with the fluorescent dye CMG, particularly when applied at a concentration of 100 ng/mL, as in our study (Midekessa et al. 2021). This resulted in only 10%–20% of LS-NTA vesicles being detected by F-NTA (Midekessa et al. 2021). Possibly, the selective insertion of the CMG fluorophore in the lipid bilayer is influenced by the unique lipid composition of SF-EVs (Arienti et al. 1998; Arvidson et al. 1989; Midekessa et al. 2021). In general, CMG labelling ratios of EVs obtained from biological fluids may vary distinctively compared to cell culture derived EVs, due to fundamental differences in tissue lipid composition (Midekessa et al. 2021). Additionally, LS-NTA displays lower specificity compared to F-NTA as it also detects non-EV particles such as lipoproteins and protein aggregates (Pasalic et al. 2016; Lu et al. 2016). In our own experiments, the high particle-to-protein ratio suggests a sufficient purity of the SF-EV stocks (Hirschberg et al. 2022; Webber and Clayton 2013). Furthermore, our isolation and purification method delivered relatively high SF-EV concentrations (6.6×10^{14} vesicles/mL based on F-NTA), likely contributing to their high stability during storage.

We investigated the characteristics and nature of trypsin-like enzyme activity in the SF-EVs considering the previously proven occurrence of TMPRSS2 at the protein level (Utleg et al. 2003; Zhang et al. 2020; Manouchehri Doulabi et al. 2022; Yang et al. 2017). A high and stable trypsin-like activity was measured in the SF-EV isolates, suggesting the presence of TMPRSS2 in SF-EVs. Many other proteases have been identified in SF-EVs at the protein level, but they either possess different substrate

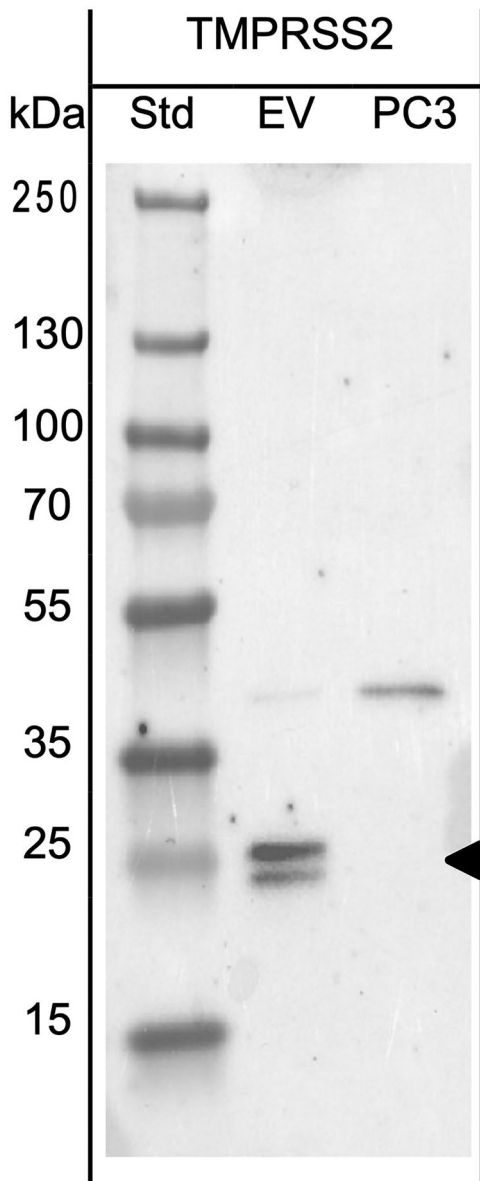


FIGURE 5 | Detection of TMPRSS2 in the seminal fluid-derived extracellular vesicle preparations. The detected TMPRSS2 band perfectly matches the theoretical weight of the Peptidase S1 domain (26 kDa) as calculated with ExPASy ProtParam, with the less prominent band probably arising due to off-target auto-activation of the protein (Gasteiger et al. 2005). The band detected in the PC3 cells most closely correlates to the extracellular topological domain of TMPRSS2 and can also slightly be detected in the SF-EVs. A molecular weight ladder (Std) was loaded on each gel. Std, PageRuler Plus Prestained Protein Ladder; EV, seminal-fluid extracellular vesicles; PC3, prostate cancer cell lysate.

specificities (e.g., PSA) or are unanchored secreted proteases (e.g., KLK2, PRSS1) that are likely removed during the purification process (Utleg et al. 2003; Coombs et al. 1998). The closest relative, Prostatin, might be present on the SF-EVs. However, we anticipate its potential interference to be minimal based on our inhibition studies. As reported in the literature, significant inhibition (>50%) of human PRSS8 is only achieved at a concentration of 0.5 μ M Nafamostat mesylate (Nimishakavi et al. 2015). Given that the IC_{50} towards the SF-EVs is significantly lower

(subnanomolar range) than that reported for PRSS8, we conclude that TMPRSS2 is the major determinant of trypsin-like enzymatic activity in SF-EVs.

The hydrolysis of the fluorogenic Boc-QAR-AMC followed classical Michaelis-Menten kinetics. The relatively broad range for the apparent K_m could be attributed to the more complex SF-EV matrix, compared to a purified recombinant protein. The IC_{50} of the serine protease inhibitor Nafamostat mesylate, a compound often used as a reference TMPRSS2 inhibitor, was within the expected range for TMPRSS2 when using SF-EVs as enzyme source, corroborating literature (Figure 3B) (Mahoney et al. 2021; Shrimp et al. 2020). Soluble TMPRSS2 freely floating in semen is expected to be limited as the shedding of TMPRSS2 into the extracellular milieu has been reported to occur at low levels (Chen et al. 2010). In our SF-EV stocks, soluble TMPRSS2 and other extravesicular proteases are largely removed during purification steps such as ultracentrifugation and size-exclusion chromatography (SEC). A minority of free TMPRSS2 may detach from the SF-EVs during storage or the assay itself. Importantly, in our hands, this does not influence our assay, as illustrated by the linear AMC increase over the assay time course.

To further validate TMPRSS2's association with SF-EVs, we performed SEC on thawed SF-EVs, demonstrating that 99% of TMPRSS2 remained vesicle-bound after a single freeze-thaw cycle. This corroborates our flow cytometry findings and results reported by Chen et al. (2010). Multiple freeze-thaw cycles, however, are likely to cause greater detachment of TMPRSS2, consistent with the lower peak absorption observed with increased freeze-thaw cycles (Figure S2A). Only after ultracentrifugation of thawed SF-EVs, 30% \pm 3% of TMPRSS2 detached from the SF-EVs. Together, these results confirm that the majority of TMPRSS2 remains associated with SF-EVs under typical assay conditions, supporting its use as a source of active TMPRSS2 in a physiologically relevant format. For other experimental applications requiring exclusively vesicle-bound TMPRSS2, we recommend an additional size-exclusion chromatography or bottom-up centrifugation step, as performed for flow cytometry, to remove any free proteins from the SF-EV samples.

In pursuit of an alternative enzyme source to validate our findings on trypsin-like enzyme activity in SF-EVs, we produced and characterised the human TMPRSS2 ectodomain in a mammalian expression system. Various strategies were attempted to express the TMPRSS2 ectodomain containing the LDLR-A, SRCR and SP subdomains in Freestyle 293-F cells. However, pilot experiments suffered from auto-degradation of the protein during the purification process. Through optimisation of production and purification steps, we successfully obtained highly active human TMPRSS2 with equal to enhanced enzymatic activity relative to previously published data (Lucas et al. 2014; Wettstein et al. 2022; Fraser et al. 2022; Shrimp et al. 2020). We attribute the high enzymatic activity due to (i) the optimal posttranslational modifications (e.g., N-glycosylation of Asn²¹³ and Asn²⁴⁹) and (ii) the prime protein folding by mammalian chaperone proteins and folding machinery. The catalytic parameters K_m , k_{cat} and V_{max} , as well as the inhibition characteristics by serine protease inhibitor Nafamostat mesylate closely resemble those of natural TMPRSS2, and reports in recent literature (Mahoney et al. 2021; Shrimp et al. 2020). Any differences observed are likely attributable to

specific assay conditions. More importantly, they indicate that the SF-EV-associated TMPRSS2 is catalytically similar to rTMPRSS2. Additionally, the successful mammalian recombinant TMPRSS2 production opens up the opportunity to further study the conformational behaviour of human TMPRSS2 with its ligands. However, our recombinant production process still suffers from low yield and a limited stability of the purified protein at 4°C. Considering cost-benefit analysis, the SF-EVs remain strongly favoured as it takes more time and reagents to obtain recombinant TMPRSS2 compared to pure SF-EVs.

CD26 was previously found to be strongly expressed on SF-EVs as well as on the luminal surface of benign prostatic epithelial cells and on the surface of prostate cancer cells in nearly 100% of the cases (Vanhoof et al. 1992; Dinjens et al. 1990). Indeed, following optimisation of the immunostaining conditions (Welsh et al. 2023), roughly 11% of CFDA-SE⁺ SF-EVs were double positive for CD26, consistent with previous reports in humans (Carlsson et al. 2006; Arienti et al. 1997). So far, TMPRSS2 in SF-EVs has only scarcely been described, despite clear indications about its expression on prostate epithelial cells (Song et al. 2020). We found that approximately 25% of CFDA-SE⁺ SF-EVs were positive for TMPRSS2. Since the semen samples used to prepare the pooled SF-EV preparations originated from fertility clinics, we believe that TMPRSS2 is constitutively present in part of the SF-EVs secreted by apparently healthy prostate epithelial cells. The modest positivity rate of TMPRSS2 on SF-EVs in our high-sensitivity flow cytometry study may stem from several factors. First and foremost, only the prostate and epididymis are described with high TMPRSS2 protein expression according to the Human Protein Atlas (www.proteinatlas.org), while the SF-EV population probably also contain extracellular vesicles from other male tissues (Uhlén et al. 2015; Cao et al. 2021). Additionally, in conjunction with the inherent heterogeneity of SF-EVs in our healthy donors, the secretion of SF-EVs from prostatic epithelial cells fluctuates depending on their current state, potentially impacting TMPRSS2 translocation into these SF-EVs (Lin et al. 1999; Zijlstra and Stoorvogel 2016). Some TMPRSS2 may also have been lost during storage at -20°C in the fertility clinics or due to the ultracentrifugation step in the purification procedure, further influencing the observed positivity rate. Furthermore, the positive correlation between TMPRSS2 intensity and SF-EV diameter (Figure S6) provides further support for the observed rate of TMPRSS2 positivity. Our HS-FCM method might overlook TMPRSS2 positivity on small EVs measuring below 90 nm and/or with dim CFDA fluorescence intensity, thus potentially influencing the observed TMPRSS2 positivity rate. Further research is needed to map the specific variations in numbers and characteristics of secreted SF-EV populations, as we used SF-EVs that had been stored for an extended period at -20°C and were pooled from multiple samples. This pooling likely reduced variation, as reflected in the comparable TMPRSS2 enzyme activities of different batches (Tables S12 and S13), but may not fully represent the heterogeneity and level of the activity observed in individual semen samples, either fresh or stored at lower temperature (-80°C) for shorter time periods (less than 1 year). Further investigation on individual semen samples is required to unravel the specific role of TMPRSS2 as part of the SF-EV surface interactome in health and malignancy (Buzás et al. 2018). Through several strategies, SF-EVs are thought to contribute to the pathogenesis of prostate cancer via immune

evasion, enhancement of local tumour invasion and promotion of bone metastasis (Tompkins et al. 2015). We hope that our proof of surface-exposed enzymatically active TMPRSS2 can help unraveling its specific role on SF-EVs, and open up opportunities to exploit SF-EVs as potential biomarkers in prostate cancer, complementing the limited predictive value of PSA screening biomarkers (Park et al. 2016; Chen et al. 2010).

Based on our demonstration that (i) intact, non-lysed SF-EVs intrinsically possess trypsin-like enzymatic activity, characteristic for TMPRSS2; (ii) this protein is presented on the SF-EV surface and (iii) SF-EVs can reliably identify potent TMPRSS2 inhibitors, we designed an in vitro screening assay for TMPRSS2-targeting compounds. We successfully adapted the assay to a 384-well plate format, maintaining robust performance. Upon further determination of its dynamic range and validation, our in vitro screening assay using SF-EVs holds promise for future drug discovery, as it offers a cost-effective platform to screen and identify TMPRSS2-inhibitors based on a native target format.

To conclude, we established enzymatically active TMPRSS2 on SF-EVs and leveraged this discovery to develop a robust biochemical screening assay for identifying compounds that target TMPRSS2 enzyme activity.

Author Contributions

Emile Verhulst: Conceptualization (equal); formal analysis (equal); investigation (equal); methodology (equal); project administration (equal); validation (equal); visualization (equal); writing—original draft (equal); writing—review and editing (equal). **Michelle De Bruyn:** Conceptualization (equal); investigation (equal); methodology (equal); writing—review and editing (equal). **Pascale Berckmans:** Formal analysis (equal); investigation (equal); validation (equal); visualization (equal); writing—review and editing (equal). **Yani Sim:** Investigation (equal); writing—review and editing (equal). **Koen Augustyns:** Resources (equal); writing—review and editing (equal). **Isabel Pintelon:** Formal analysis (equal); investigation (equal); validation (equal); visualization (equal); writing—review and editing (equal). **Maya Berg:** Funding acquisition (equal); project administration (equal); writing—review and editing (equal). **Pieter Van Wielendaele:** Methodology (equal); writing—review and editing (equal). **Anne-Marie Lambeir:** Formal analysis (equal); validation (equal); writing—review and editing (equal). **Yann G.-J. Sterckx:** Funding acquisition (equal); resources (equal); supervision (equal); writing—review and editing (equal). **Inge Nelissen:** Conceptualization (equal); formal analysis (equal); funding acquisition (equal); investigation (equal); methodology (equal); resources (equal); supervision (equal); validation (equal); writing—review and editing (equal). **Ingrid De Meester:** Conceptualization (equal); funding acquisition (equal); methodology (equal); project administration (equal); resources (equal); supervision (equal); validation (equal); writing—original draft (equal); writing—review and editing (equal).

Acknowledgements

The authors thank Kris Peeters for valuable advice and the Flemish Fertility Clinics for providing the anonymous leftover semen samples. The authors thank Karen Sterck and Elien Theuns of the Laboratory of Cell Biology and Histology (University of Antwerp) for their technical assistance with the transmission electron microscopy experiments, and An Jacobs and Rebekka Van Hoof of the Flemish Institute for Technological Research (VITO) for their technical assistance with the NTA experiments. The authors thank the laboratory members of the Center for Oncological Research (University of Antwerp) for the batch of cryopreserved PC-3

cells. This work was supported by the University Research Council (BOF) Antwerp under Grant number 45146 (EVZYM project) and VITO.

Conflicts of Interest

The authors declare that they have no known competing financial interests or personal relationships that could have appeared to influence the work reported in this paper.

References

- Abe, M., M. Tahara, K. Sakai, et al. 2013. "TMPRSS2 is an Activating Protease for Respiratory Parainfluenza Viruses." *Journal of Virology* 87: 11930–11935.
- Afar, D. E., I. Vivanco, R. S. Hubert, et al. 2001. "Catalytic Cleavage of the Androgen-Regulated TMPRSS2 Protease Results in Its Secretion by Prostate and Prostate Cancer Epithelia." *Cancer Research* 61: 1686–1692.
- Arienti, G., E. Carlini, A. Polci, E. V. Cosmi, and C. A. Palmerini. 1998. "Fatty Acid Pattern of Human Prostate Lipid." *Archives of Biochemistry and Biophysics* 358: 391–395.
- Arienti, G., A. Polci, E. Carlini, and C. A. Palmerini. 1997. "Transfer of CD26/Dipeptidyl Peptidase IV (E.C. 3.5.4.4) From Prostate to Sperm." *FEBS Letters* 410: 343–346.
- Arvidson, G., G. Ronquist, G. Wikander, and A.-C. Öjteg. 1989. "Human Prostate Membranes Exhibit Very High Cholesterol/Phospholipid Ratios Yielding High Molecular Ordering." *Biochimica Et Biophysica Acta (BBA)—Biomembranes* 984: 167–173.
- Bertram, S., I. Glowacka, P. Blazejewska, et al. 2010. "TMPRSS2 and TMPRSS4 Facilitate Trypsin-Independent Spread of Influenza Virus in Caco-2 Cells." *Journal of Virology* 84: 10016–10025.
- Bertram, S., A. Heurich, H. Lavender, et al. 2012. "Influenza and SARS-Coronavirus Activating Proteases TMPRSS2 and HAT Are Expressed at Multiple Sites in Human Respiratory and Gastrointestinal Tracts." *PLoS ONE* 7: e35876.
- Bestle, D., M. R. Heindl, H. Limburg, et al. 2020. "TMPRSS2 and Furin Are Both Essential for Proteolytic Activation of SARS-CoV-2 in Human Airway Cells." *Life Science Alliance* 3, no. 9: e202000786.
- Bestle, D., H. Limburg, D. Kruhl, et al. 2021. "Hemagglutinins of Avian Influenza Viruses Are Proteolytically Activated by TMPRSS2 in Human and Murine Airway Cells." *Journal of Virology* 95: e0090621.
- Bohren C. F., and D. R. Huffman. 2007. "Absorption and Scattering by a Sphere." In *Absorption and Scattering of Light by Small Particles*, 83–129. Wiley-VCH Verlag GmbH.
- Böttcher, E., T. Matrosovich, M. Beyerle, H. D. Klenk, W. Garten, and M. Matrosovich. 2006. "Proteolytic Activation of Influenza Viruses by Serine Proteases TMPRSS2 and HAT From Human Airway Epithelium." *Journal of Virology* 80: 9896–9898.
- Bradford, M. M. 1976. "A Rapid and Sensitive Method for the Quantitation of Microgram Quantities of Protein Utilizing the Principle of Protein-Dye Binding." *Analytical Biochemistry* 72: 248–254.
- Brody, I., G. Ronquist, and A. Gottfries. 1983. "Ultrastructural Localization of the Prostate—An Organelle in Human Seminal Plasma." *Upsala Journal of Medical Sciences* 88: 63–80.
- Bugge, T. H., T. M. Antalis, and Q. Wu. 2009. "Type II Transmembrane Serine Proteases." *Journal of Biological Chemistry* 284: 23177–23181.
- Buzás, E. I., E. Tóth, B. W. Sódar, and K. Szabó-Taylor. 2018. "Molecular Interactions at the Surface of Extracellular Vesicles." *Seminars in Immunopathology* 40: 453–464.
- Cao, W., Q. Feng, and X. Wang. 2021. "Computational Analysis of TMPRSS2 Expression in Normal and SARS-CoV-2-Infected Human Tissues." *Chemico-Biological Interactions* 346: 109583.
- Carlsson, L., O. Nilsson, A. Larsson, M. Stridsberg, G. Sahlén, and G. Ronquist. 2003. "Characteristics of Human Prostate Isolated From Three Different Sources." *Prostate* 54: 322–330.
- Carlsson, L., C. Pålsson, M. Bergquist, G. Ronquist, and M. Stridsberg. 2000. "Antibacterial Activity of Human Prostate." *Prostate* 44: 279–286.
- Carlsson, L., G. Ronquist, R. Eliasson, N. Egberg, and A. Larsson. 2006. "Flow Cytometric Technique for Determination of Prostate Quantity, Size and Expression of CD10, CD13, CD26 and CD59 in Human Seminal Plasma." *International Journal of Andrology* 29: 331–338.
- Chen, Y.-W., M. S. Lee, A. Lucht, et al. 2010. "TMPRSS2, a Serine Protease Expressed in the Prostate on the Apical Surface of Luminal Epithelial Cells and Released Into Semen in Prostate, Is Misregulated in Prostate Cancer Cells." *American Journal of Pathology* 176: 2986–2996.
- Clausen, T. M., D. R. Sandoval, C. B. Spliid, et al. 2020. "SARS-CoV-2 Infection Depends on Cellular Heparan Sulfate and ACE2." *Cell* 183: 1043–1057.e1015.
- Coombs, G. S., R. C. Bergstrom, J. L. Pellequer, et al. 1998. "Substrate Specificity of Prostate-Specific Antigen (PSA)." *Chemistry & Biology* 5: 475–488.
- Daly, J. L., B. Simonetti, K. Klein, et al. 2020. "Neuropilin-1 Is a Host Factor for SARS-CoV-2 Infection." *Science* 370: 861–865.
- De Bruyn, M. 2022. "Profiling of proteases as potential therapeutic targets: Focus on inflammatory bowel disease (IBD) and irritable bowel disease (IBS)." In *Faculty of Pharmaceutical, Biomedical and Veterinary Sciences*, University of Antwerp.
- De Meester, I., G. Vanhoof, A.-M. Lambeir, and S. Scharpé. 1996. "Use of Immobilized Adenosine Deaminase (EC 3.5.4.4) for the Rapid Purification of Native Human CD26/Dipeptidyl Peptidase IV (EC 3.4.14.5)." *Journal of Immunological Methods* 189: 99–105.
- Deville, S., P. Berckmans, R. Van Hoof, I. Lambrichts, A. Salvati, and I. Nelissen. 2021. "Comparison of Extracellular Vesicle Isolation and Storage Methods Using High-Sensitivity Flow Cytometry." *PLoS ONE* 16: 1–17.
- Dinjens, W. N. M., J. Ten Kate, J. A. Kirch, et al. 1990. "Adenosine Deaminase Complexing Protein (ADCP) Expression and Metastatic Potential in Prostatic Adenocarcinomas." *Journal of Pathology* 160: 195–201.
- Donaldson, S. H., A. Hirsh, D. C. Li, et al. 2002. "Regulation of the Epithelial Sodium Channel by Serine Proteases in Human Airways*." *Journal of Biological Chemistry* 277: 8338–8345.
- Dragovic, R. A., C. Gardiner, A. S. Brooks, et al. 2011. "Sizing and Phenotyping of Cellular Vesicles Using Nanoparticle Tracking Analysis." *Nanomedicine: Nanotechnology, Biology and Medicine* 7: 780–788.
- Dubois, L., K. K. G. Ronquist, B. Ek, G. Ronquist, and A. Larsson. 2015. "Proteomic Profiling of Detergent Resistant Membranes (Lipid Rafts) of Prostate." *Molecular & Cellular Proteomics: MCP* 14: 3015–3022.
- Dubois, V., A. M. Lambeir, P. Van der Veken, et al. 2008. "Purification and Characterization of Dipeptidyl Peptidase IV-Like Enzymes From Bovine Testes." *Frontiers in Bioscience-Landmark* 13: 3558–3568.
- Duijvesz, D., T. Luider, C. H. Bangma, and G. Jenster. 2011. "Exosomes as Biomarker Treasure Chests for Prostate Cancer." *European Urology* 59: 823–831.
- Esumi, M., M. Ishibashi, H. Yamaguchi, et al. 2015. "Transmembrane Serine Protease TMPRSS2 Activates Hepatitis C Virus Infection." *Hepatology* 61: 437–446.
- Fraser, B. J., S. Beldar, A. Seitova, et al. 2022. "Structure and Activity of Human TMPRSS2 Protease Implicated in SARS-CoV-2 Activation." *Nature Chemical Biology* 18: 963–971.
- Gasteiger E., A. H. C. Gattiker, S. Duvaud, M. R. Wilkins, R. D. Appel, and A. Bairoch. 2005. "Protein Identification and Analysis Tools on the ExPASy Server." In *The Proteomics Protocols Handbook*, edited by J. M. Walker, 1st ed., 571–607. Humana Totowa.
- Gkogkou, E., G. Barnasas, K. Vougas, and I. P. Trougakos. 2020. "Expression Profiling Meta-Analysis of ACE2 and TMPRSS2, the Putative Anti-Inflammatory Receptor and Priming Protease of SARS-CoV-2 in Human Cells, and Identification of Putative Modulators." *Redox Biology* 36: 101615.

- Glowacka, I., S. Bertram, M. A. Müller, et al. 2011. "Evidence That TMPRSS2 Activates the Severe Acute Respiratory Syndrome Coronavirus Spike Protein for Membrane Fusion and Reduces Viral Control by the Humoral Immune Response." *Journal of Virology* 85: 4122–4134.
- Groot Kormelink, T., G. J. Arkesteijn, F. A. Nauwelaers, G. van den Engh, E. N. Nolte-'t Hoen, and M. H. Wauben. 2016. "Prerequisites for the Analysis and Sorting of Extracellular Vesicle Subpopulations by High-Resolution Flow Cytometry." *Cytometry Part A: The Journal of the International Society for Analytical Cytology* 89: 135–147.
- Hirschberg, Y., K. Boonen, K. Schildermans, et al. 2022. "Characterising Extracellular Vesicles From Individual Low Volume Cerebrospinal Fluid Samples, Isolated by SmartSEC." *Journal of Extracellular Biology* 1: e55.
- Hoffmann, M., H. Hofmann-Winkler, J. C. Smith, et al. 2021. "Camostat Mesylate Inhibits SARS-CoV-2 Activation by TMPRSS2-Related Proteases and Its Metabolite GBPA Exerts Antiviral Activity." *EBioMedicine* 65: 103255.
- Hoffmann, M., H. Kleine-Weber, and S. A. Pöhlmann. 2020. "Multibasic Cleavage Site in the Spike Protein of SARS-CoV-2 Is Essential for Infection of Human Lung Cells." *Molecular Cell* 78: 779–784.
- Hoffmann, M., H. Kleine-Weber, S. Schroeder, et al. 2020. "SARS-CoV-2 Cell Entry Depends on ACE2 and TMPRSS2 and Is Blocked by a Clinically Proven Protease Inhibitor." *Cell* 181: 271–280.e8.
- Jacquinet, E., N. V. Rao, G. V. Rao, W. Zhengming, K. H. Albertine, and J. R. Hoidal. 2001. "Cloning and Characterization of the cDNA and Gene for Human Epitheliasin." *European Journal of Biochemistry* 268: 2687–2699.
- Kelly, R. W. 1995. "Immunosuppressive Mechanisms in Semen: Implications for Contraception." *Human Reproduction* 10: 1686–1693.
- Kelly, R. W., P. Holland, G. Skibinski, et al. 1991. "Extracellular Organelles (Prostasomes) Are Immunosuppressive Components of Human Semen." *Clinical and Experimental Immunology* 86: 550–556.
- Kim, T. S., C. Heinlein, R. C. Hackman, and P. S. Nelson. 2006. "Phenotypic Analysis of Mice Lacking the *Tmprss2*-Encoded Protease." *Molecular and Cellular Biology* 26: 965–975.
- Kitamura, M., M. Namiki, K. Matsumiya, et al. 1995. "Membrane Cofactor Protein (CD46) in Seminal Plasma Is a Prostate-Bound Form With Complement Regulatory Activity and Measles Virus Neutralizing Activity." *Immunology* 84: 626–632.
- Kleine-Weber, H., M. T. Elzayat, M. Hoffmann, and S. Pöhlmann. 2018. "Functional Analysis of Potential Cleavage Sites in the MERS-Coronavirus Spike Protein." *Scientific Reports* 8: 16597.
- Ko, C.-J., C. C. Huang, H. Y. Lin, et al. 2015. "Androgen-Induced TMPRSS2 Activates Matriptase and Promotes Extracellular Matrix Degradation, Prostate Cancer Cell Invasion, Tumor Growth, and Metastasis." *Cancer Research* 75: 2949–2960.
- Laporte, M., and L. Naesens. 2017. "Airway Proteases: An Emerging Drug Target for Influenza and Other Respiratory Virus Infections." *Current Opinion in Virology* 24: 16–24.
- Li, F., M. Han, P. Dai, et al. 2021. "Distinct Mechanisms for TMPRSS2 Expression Explain Organ-Specific Inhibition of SARS-CoV-2 Infection by Enzalutamide." *Nature Communications* 12: 866.
- Lilja, H., and C.-B. Laurell. 1984. "Liquefaction of Coagulated Human Semen." *Scandinavian Journal of Clinical and Laboratory Investigation* 44: 447–452.
- Lin, B., C. Ferguson, J. T. White, et al. 1999. "Prostate-Localized and Androgen-Regulated Expression of the Membrane-Bound Serine Protease TMPRSS2." *Cancer Research* 59: 4180–4184.
- Lu, J.-C., J. Jing, Q. Yao, et al. 2016. "Relationship Between Lipids Levels of Serum and Seminal Plasma and Semen Parameters in 631 Chinese Subfertile Men." *PLoS ONE* 11: e0146304.
- Lucas, J. M., C. Heinlein, T. Kim, et al. 2014. "The Androgen-Regulated Protease TMPRSS2 Activates a Proteolytic Cascade Involving Components of the Tumor Microenvironment and Promotes Prostate Cancer Metastasis." *Cancer Discovery* 4: 1310–1325.
- Lukassen S., R. L. Chua, T. Trefzer, et al. 2020. "SARS-CoV-2 Receptor ACE2 and TMPRSS2 Are Primarily Expressed in Bronchial Transient Secretory Cells." *EMBO Journal* 39: e105114.
- Mahoney, M., V. C. Damalanka, M. A. Tartell, et al. 2021. "A Novel Class of TMPRSS2 Inhibitors Potently Block SARS-CoV-2 and MERS-CoV Viral Entry and Protect Human Epithelial Lung Cells." *Proceedings of the National Academy of Sciences* 118: e2108728118.
- Manouchehri Doulabi, E., C. Fredolini, R. Gallini, et al. 2022. "Surface Protein Profiling of Prostate-Derived Extracellular Vesicles by Mass Spectrometry and Proximity Assays." *Communications Biology* 5: 1402.
- Matheeussen, V., A. M. Lambeir, W. Jungraithmayr, et al. 2012. "Method Comparison of Dipeptidyl Peptidase IV Activity Assays and Their Application in Biological Samples Containing Reversible Inhibitors." *Clinica Chimica Acta* 413: 456–462.
- Matsuyama, S., N. Nagata, K. Shirato, M. Kawase, M. Takeda, and F. Taguchi. 2010. "Efficient Activation of the Severe Acute Respiratory Syndrome Coronavirus Spike Protein by the Transmembrane Protease TMPRSS2." *Journal of Virology* 84: 12658–12664.
- Meyer, D., F. Sielaff, M. Hammami, E. Böttcher-Friebertshäuser, W. Garten, and T. Steinmetzer. 2013. "Identification of the First Synthetic Inhibitors of the Type II Transmembrane Serine Protease TMPRSS2 Suitable for Inhibition of Influenza Virus Activation." *Biochemical Journal* 452: 331–343.
- Midekessa, G., K. Godakumara, K. Dissanayake, et al. 2021. "Characterization of Extracellular Vesicles Labelled With a Lipophilic Dye Using Fluorescence Nanoparticle Tracking Analysis." *Membranes (Basel)* 11: 779.
- Nimishakavi, S., W. W. Raymond, D. C. Gruenert, and G. H. Caughey. 2015. "Divergent Inhibitor Susceptibility Among Airway Lumen-Accessible Trypsin Proteases." *PLoS ONE* 10: e0141169.
- Palmerini, C. A., C. Saccardi, E. Carlini, R. Fabiani, and G. Arienti. 2003. "Fusion of Prostasomes to Human Spermatozoa Stimulates the Acrosome Reaction." *Fertility and Sterility* 80: 1181–1184.
- Paoloni-Giacobino, A., H. Chen, M. C. Peitsch, C. Rossier, and S. E. Antonarakis. 1997. "Cloning of the TMPRSS2 Gene, Which Encodes a Novel Serine Protease With Transmembrane, LDLRA, and SRCR Domains and Maps to 21q22.3." *Genomics* 44: 309–320.
- Park, Y. H., H. W. Shin, A. R. Jung, et al. 2016. "Prostate-Specific Extracellular Vesicles as a Novel Biomarker in Human Prostate Cancer." *Scientific Reports* 6: 30386.
- Pasalic, L., R. Williams, A. Siupa, H. Campbell, M. J. Henderson, and V. M. Y. Chen. 2016. "Enumeration of Extracellular Vesicles by a New Improved Flow Cytometric Method Is Comparable to Fluorescence Mode Nanoparticle Tracking Analysis." *Nanomedicine: Nanotechnology, Biology and Medicine* 12: 977–986.
- Pawar, N. R., M. S. Buzza, and T. M. Antalis. 2019. "Membrane-Anchored Serine Proteases and Protease-Activated Receptor-2-Mediated Signaling: Co-Conspirators in Cancer Progression." *Cancer Research* 79: 301–310.
- Poliakov, A., M. Spilman, T. Dokland, C. L. Amling, and J. A. Mobley. 2009. "Structural Heterogeneity and Protein Composition of Exosome-Like Vesicles (Prostasomes) in Human Semen." *Prostate* 69: 159–167.
- Pons-Rejraji, H., C. Artonne, B. Sion, et al. 2011. "Prostasomes: Inhibitors of Capacitation and Modulators of Cellular Signalling in Human Sperm." *International Journal of Andrology* 34: 568–580.
- Renneberg, H., M. Albrecht, R. Kurek, et al. 2001. "Identification and Characterization of Neutral Endopeptidase (EC 3. 4. 24. 11) From Human Prostasomes—Localization in Prostatic Tissue and Cell Lines." *Prostate* 46: 173–183.
- Roca, J., H. Rodriguez-Martinez, L. Padilla, X. Lucas, and I. Barranco. 2022. "Extracellular Vesicles in Seminal Fluid and Effects on Male Reproduction. An Overview in Farm Animals and Pets." *Animal Reproduction Science* 246: 106853.
- Ronquist, G. 2012. "Prostasomes Are Mediators of Intercellular Communication: From Basic Research to Clinical Implications." *Journal of Internal Medicine* 271: 400–413.

- Ronquist, G., and I. Brody. 1985. "The Prostatome: Its Secretion and Function in Man." *Biochimica Et Biophysica Acta* 822: 203–218.
- Rooney, I. A., J. P. Atkinson, E. S. Krul, et al. 1993. "Physiologic Relevance of the Membrane Attack Complex Inhibitory Protein CD59 in Human Seminal Plasma: CD59 Is Present on Extracellular Organelles (Prostatomes), Binds Cell Membranes, and Inhibits Complement-Mediated Lysis." *Journal of Experimental Medicine* 177: 1409–1420.
- Sahlén, G. E., L. Egevad, A. Ahlander, B. J. Norlén, G. Ronquist, and B. O. Nilsson. 2002. "Ultrastructure of the Secretion of Prostatomes From Benign and Malignant Epithelial Cells in the Prostate." *Prostate* 53: 192–199.
- Sakai, K., Y. Ami, M. Tahara, et al. 2014. "The Host Protease TMPRSS2 Plays a Major Role in In Vivo Replication of Emerging H7N9 and Seasonal Influenza Viruses." *Journal of Virology* 88: 5608–5616.
- Sarker, J., P. Das, S. Sarker, A. K. Roy, and A. Z. M. R. Momen. 2021. "A Review on Expression, Pathological Roles, and Inhibition of TMPRSS2, the Serine Protease Responsible for SARS-CoV-2 Spike Protein Activation." *Scientifica* 2021: 2706789.
- Saunders, N., I. Fernandez, C. Planchais, et al. 2023. "TMPRSS2 is a Functional Receptor for Human Coronavirus HKU1." *Nature* 624, no. 7990: 207–214.
- Schneider, W. M., J. M. Luna, H. H. Hoffmann, et al. 2021. "Genome-Scale Identification of SARS-CoV-2 and Pan-Coronavirus Host Factor Networks." *Cell* 184: 120–132.e114.
- Shirato, K., M. Kawase, and S. Matsuyama. 2013. "Middle East Respiratory Syndrome Coronavirus Infection Mediated by the Transmembrane Serine Protease TMPRSS2." *Journal of Virology* 87: 12552–12561.
- Shirogane, Y., M. Takeda, M. Iwasaki, et al. 2008. "Efficient Multiplication of Human Metapneumovirus in Vero Cells Expressing the Transmembrane Serine Protease TMPRSS2." *Journal of Virology* 82: 8942–8946.
- Shrimp, J. H., S. C. Kales, P. E. Sanderson, A. Simeonov, M. Shen, and M. D. Hall. 2020. "An Enzymatic TMPRSS2 Assay for Assessment of Clinical Candidates and Discovery of Inhibitors as Potential Treatment of COVID-19." *ACS Pharmacology & Translational Science* 3: 997–1007.
- Siciliano, L., V. Marcianò, and A. Carpino. 2008. "Prostatome-Like Vesicles Stimulate Acrosome Reaction of Pig Spermatozoa." *Reproductive Biology and Endocrinology* 6: 5.
- Skotland, T., N. P. Hessvik, K. Sandvig, and A. Llorente. 2019. "Exosomal Lipid Composition and the Role of Ether Lipids and Phosphoinositides in Exosome Biology." *Journal of Lipid Research* 60: 9–18.
- Song, H., B. Seddighzadeh, M. R. Cooperberg, and F. W. Huang. 2020. "Expression of ACE2, the SARS-CoV-2 Receptor, and TMPRSS2 in Prostate Epithelial Cells." *European Urology* 78: 296–298.
- Stegmayr, B., and G. Ronquist. 1982. "Promotive Effect on Human Sperm Progressive Motility by Prostatomes." *Urological Research* 10: 253–257.
- Tanase, C. P., E. Codrici, I. D. Popescu, et al. 2017. "Prostate Cancer Proteomics: Current Trends and Future Perspectives for Biomarker Discovery." *Oncotarget* 8: 18497–18512.
- Théry, C., K. W. Witwer, E. Aikawa, et al. 2018. "Minimal Information for Studies of Extracellular Vesicles 2018 (MISEV2018): A Position Statement of the International Society for Extracellular Vesicles and Update of the MISEV2014 Guidelines." *Journal of Extracellular Vesicles* 7: 153750.
- Thunders, M., and B. Delahunt. 2020. "Gene of the Month: TMPRSS2 (Transmembrane Serine Protease 2)." *Journal of Clinical Pathology* 73: 773–776.
- Tompkins, A. J., D. Chatterjee, M. Maddox, et al. 2015. "The Emergence of Extracellular Vesicles in Urology: Fertility, Cancer, Biomarkers and Targeted Pharmacotherapy." *Journal of Extracellular Vesicles* 4: 23815.
- Trajkovic, K., C. Hsu, S. Chiantia, et al. 2008. "Ceramide Triggers Budding of Exosome Vesicles Into Multivesicular Endosomes." *Science* 319: 1244–1247.
- Troisi, A., M. Schrank, I. Bellezza, et al. 2023. "Expression of CD13 and CD26 on Extracellular Vesicles in Canine Seminal Plasma: Preliminary Results." *Veterinary Research Communications* 48, no. 1: 357–366.
- Uhlén, M., L. Fagerberg, B. M. Hallström, et al. 2015. "Tissue-Based Map of the Human Proteome." *Science* 347: 1260419.
- Utleig, A. G., E. C. Yi, T. Xie, et al. 2003. "Proteomic Analysis of Human Prostatomes." *Prostate* 56: 150–161.
- Vaarala, M. H., K. Porvari, A. Kyllönen, O. Lukkarinen, and P. Vihko. 2001. "The TMPRSS2 Gene Encoding Transmembrane Serine Protease Is Overexpressed in a Majority of Prostate Cancer Patients: Detection of Mutated TMPRSS2 Form in a Case of Aggressive Disease." *International Journal of Cancer* 94: 705–710.
- Vaarala, M. H., K. S. Porvari, S. Kellokumpu, A. P. Kyllönen, and P. T. Vihko. 2001. "Expression of Transmembrane Serine Protease TMPRSS2 in Mouse and Human Tissues." *Journal of Pathology* 193: 134–140.
- Van Deun, J., P. Mestdagh, P. Agostinis, et al. 2017. "EV-TRACK: Transparent Reporting and Centralizing Knowledge in Extracellular Vesicle Research." *Nature Methods* 14: 228–232.
- Vanhoof, G., I. De Meester, M. van Sande, S. Scharpé, and A. Yaron. 1992. "Distribution of Proline-Specific Aminopeptidases in Human Tissues and Body Fluids." *European Journal of Clinical Chemistry and Clinical Biochemistry* 30: 333–338.
- Vickram, A. S., H. A. Samad, S. K. Latheef, et al. 2020. "Human Prostatomes an Extracellular Vesicle—Biomarkers for Male Infertility and Prostate Cancer: The Journey From Identification to Current Knowledge." *International Journal of Biological Macromolecules* 146: 946–958.
- Wang, N., X. Shi, L. Jiang, et al. 2013. "Structure of MERS-CoV Spike Receptor-Binding Domain Complexed With Human Receptor DPP4." *Cell Research* 23: 986–993.
- Wang, R., C. R. Simoneau, J. Kulsuptrakul, et al. 2021. "Genetic Screens Identify Host Factors for SARS-CoV-2 and Common Cold Coronaviruses." *Cell* 184: 106–119.e114.
- Webber, J., and A. Clayton. 2013. "How Pure Are Your Vesicles?" *Journal of Extracellular Vesicles* 2: 1–6.
- Wei, J., M. M. Alfajaro, P. C. DeWeirdt, et al. 2021. "Genome-Wide CRISPR Screens Reveal Host Factors Critical for SARS-CoV-2 Infection." *Cell* 184: 76–91.e13.
- Welsh, J. A., G. J. A. Arkesteijn, M. Bremer, et al. 2023. "A Compendium of Single Extracellular Vesicle Flow Cytometry." *Journal of Extracellular Vesicles* 12: e12299.
- Wettstein, L., F. Kirchhoff, and J. Münch. 2022. "The Transmembrane Protease TMPRSS2 as a Therapeutic Target for COVID-19 Treatment." *International Journal of Molecular Sciences* 23: 1351.
- Wilson, S., B. Greer, J. Hooper, et al. 2005. "The Membrane-Anchored Serine Protease, TMPRSS2, Activates PAR-2 in Prostate Cancer Cells." *Biochemical Journal* 388: 967–972.
- Wu, G., Y. Yuan, and C. N. Hodge. 2003. "Determining Appropriate Substrate Conversion for Enzymatic Assays in High-Throughput Screening." *Journal of Biomolecular Screening: The Official Journal of the Society for Biomolecular Screening* 8: 694–700.
- Yang, C., W. B. Guo, W. S. Zhang, et al. 2017. "Comprehensive Proteomics Analysis of Exosomes Derived From Human Seminal Plasma." *Andrology* 5: 1007–1015.
- Zang, R., M. F. Gomez Castro, B. T. McCune, et al. 2020. "TMPRSS2 and TMPRSS4 Promote SARS-CoV-2 Infection of Human Small Intestinal Enterocytes." *Science Immunology* 5, no. 47: eabc3582.
- Zhang, X., H. R. Vos, W. Tao, and W. Stoorvogel. 2020. "Proteomic Profiling of Two Distinct Populations of Extracellular Vesicles Isolated From Human Seminal Plasma." *International Journal of Molecular Sciences* 21: 7957.

Zhang, Y., S. Sun, C. Du, et al. 2022. "Transmembrane Serine Protease TMPRSS2 Implicated in SARS-CoV-2 Infection Is Autoactivated Intracellularly and Requires N-Glycosylation for Regulation." *Journal of Biological Chemistry* 298: 102643.

Zijlstra, C., and W. Stoorvogel. 2016. "Prostasomes as a Source of Diagnostic Biomarkers for Prostate Cancer." *Journal of Clinical Investigation* 126: 1144–1151.

Supporting Information

Additional supporting information can be found online in the Supporting Information section.